1-1996

Force Diagnostics of Aerodynamic Bodies Based on Wake-Plane Data

Bohus Ondrusek
University of Tennessee - Knoxville

To the Graduate Council:

I am submitting herewith a thesis written by Bohus Ondrusek entitled "Force Diagnostics of Aerodynamic Bodies Based on Wake-Plane Data." I have examined the final electronic copy of this thesis for form and content and recommend that it be accepted in partial fulfillment of the requirements for the degree of Master of Science, with a major in Aerospace Engineering.

J. M. Wu, Major Professor

We have read this thesis and recommend its acceptance:

A. Vakili, G. A. Flandro

Accepted for the Council:
Carolyn R. Hodges

Vice Provost and Dean of the Graduate School

(Original signatures are on file with official student records.)

To the Graduate Council:

I am submitting herewith a thesis written by Bohus Ondrusek entitled "Force Diagnostics of Aerodynamic Bodies Based on Wake-Plane Data." I have examined the final copy of this thesis for form and content and recommend that it be accepted in partial fulfillment of the requirements for the degree of Master of Science, with a major in Aerospace Engineering.

Dr. J.M. Wu, Major Professor

We have read this thesis
and recommend its acceptance:

Accepted for the Council:

Associate Vice Chancellor
and Dean of The Graduate School

Force Diagnostics of Aerodynamic Bodies Based on Wake-Plane Data

A Thesis

Presented for the

Master of Science

Degree

The University of Tennessee, Knoxville

Bohus Ondrusek

January 1996

Acknowledgments

There are many people to whom I am thankful for making my stay at The University of Tennessee Space Institute enjoyable and productive.

I would like to thank my thesis committee, Dr. A. Vakili and Dr. G. A. Flandro, for their time spent reviewing my report and for their educational guidance. To Dr. J.Z. Wu I extend my thanks for his great insight and guidance during my research development. I also extend my appreciation to our librarians Mary Lo and Brenda Brooks for their enthusiastic assistance, to Linda Engels for her technical support while writing this report, and to Jinsong Liu and Tiangui Zheng for their helpful discussions while working on my research topic.

I would especially like to thank my major Professor J.M. Wu for not only academic help in education and research, but also for his guidance outside of the academic scope.

On behalf of our entire group, I thank Mr. W. L. Sellers of NASA Langley Research Center for providing us with the experimental data and Mr. A.E. Washburn for his helpful discussions and suggestions.

Abstract

The conventional method of using a balance to measure lift and drag on a model in a wind tunnel only provides information about the total quantities of these force components. Wake-survey analysis is a different technique developed for determining aerodynamic force on a body. Compared with the balance measurement, it provides a great deal of information about decomposed constituents and it clarifies the source of the aerodynamic force, but it also requires considerable work. In 1989, J.Z. Wu and J.M. Wu developed a unique theory, based on vorticity, for determining sources of aerodynamic force on a body from wake-plane data. They applied an integration by parts to the original momentum balance in a control volume, and obtained an exact result expressed only in terms of the wake-plane data. In this thesis, the above theory is applied to the near-wake data behind a delta wing, obtained from NASA Langley Research Center. The total lift and drag coefficients are calculated and compared to the experimental results. Four normal force constituents and four axial force constituents are computed and plotted along the span. Finally, total lift and drag distributions along the span are determined, and aerodynamic efficiency (lift to drag ratio) is identified for various span locations.

Table of Contents

List of Figures

List of Tables

Nomenclature

$d = k + 1$	spatial dimension
b	wing span
c	wing chord
S	wing area
x, y, z	Cartesian coordinates
u, v, w	velocity components of $\boldsymbol{u}$
$\omega_x, \omega_y, \omega_z$	vorticity components of $\boldsymbol{\omega} = \boldsymbol{\nabla} \times \boldsymbol{u}$
$\bar{x}, \bar{y}, \bar{z}$	Cartesian non-dimensional coordinates, $\bar{x}_i = x_i/c$
$\bar{u}, \bar{v}, \bar{w}$	non-dimensional velocity components, $\bar{u}_i = u_i/U_\infty$
$\Omega_x, \Omega_y, \Omega_z$	non-dimensional vorticity components, $\Omega_i = \omega_i c/U_\infty$
p	static pressure
p_0	total pressure
$C_p = (p - p_\infty)/(\frac{1}{2}\rho U_\infty^2)$	static pressure coefficient
$C_{p_0} = (p_0 - p_\infty)/(\frac{1}{2}\rho U_\infty^2)$	total pressure coefficient
h	enthalpy
h_0	total enthalpy
ρ	density
s	entropy
γ	ratio of specific heats
T	temperature
$a = \sqrt{\gamma R T}$	speed of sound
Re	Reynolds Number
$M = U_\infty/a$	free stream Mach Number

M_x, M_y, M_z	local Mach Numbers in x, y, z directions respectively, $M_i = u_i/a$
α	angle of attack
$\boldsymbol{n}$	normal unit vector pointing out of control surface
$\boldsymbol{F}$	aerodynamic force
L	lift
D	drag
F_N	normal force
F_A	axial force
$C_L = L/(\frac{1}{2}\rho U_\infty^2 S)$	lift coefficient
$C_D = D/(\frac{1}{2}\rho U_\infty^2 S)$	drag coefficient
$C_{F_N} = F_N/(\frac{1}{2}\rho U_\infty^2 S)$	normal force coefficient
$C_{F_A} = F_A/(\frac{1}{2}\rho U_\infty^2 S)$	axial force coefficient
V	control volume
∂V	control surface
$U'_{\%}$	free-stream drift in %
J	number of grid points in y-direction
K	number of grid points in z-direction

Subscripts

$\mathcal{T}$	near wake plane
∞	free stream values
π	vector components in plane $\mathcal{T}$
$comp$	compressible
inc	incompressible

Chapter I

Introduction

The resistance of bodies moving in fluid, known as drag, has been a subject of continuing interest to the designers of aircrafts, ships, submarines and automobiles. Moreover, to aircraft designers, aerodynamic efficiency (lift to drag ratio) is a crucial design parameter, because high lift to drag ratio is desirable for superior designs. In the conventional measurement of aerodynamic force acting on a vehicle in a wind tunnel by using a balance, one obtains information only about the total quantities such as drag, lift, pitching moment, etc. For the purpose of diagnostics and optimization, it is desirable to decompose these total values into different constituents, each associated with a physical mechanism, in order to determine their magnitudes and signs, and to trace back their sources.

Wake survey analysis, a different technique for determining force on a body, may serve this purpose. Compared with a force measurement by a balance, it can provide a great deal of information about decomposed constituents. The first practical work in wake-plane analysis is credited to Betz [1]. In the mid 1920's, he developed a theory for determining profile drag (due to total pressure and axial velocity variations) and induced drag (due to induced cross-flow velocities) from a far-wake plane (a well-known Trefftz Plane) of incompressible flows. Later, Maskell [2] contributed to the Betz theory by computing the induced drag only from the rotational part of the wake-plane, by including the effects of tunnel boundary constraint and by pointing out Betz's omission of an axial-flow perturbation term. However, the theory was still applicable only to a far-wake plane. Because the size limitations of wind tunnel test sections make far-wake quantitative surveys impractical, it was necessary to develop

a theory applicable to a near-wake plane. In 1984, Hackett and Sugavan [3] devised methods which make the Betz-Maskell theory suitable for use in the near-wake plane of a wind tunnel model. This theory, which is approximate in nature, provides the basis for the recent quantitative wake surveys conducted by Hackett and Sugavan [3,4], Brune [5,6], and Takahashi and Ross [7].

Another first order wake-plane theory, developed by Yates and Donaldson [8], has not, to the author's knowledge, been put to use in wind tunnel applications, because of far-wake restrictions.

Because of an interest in optimal design of future aerodynamic shapes of vehicles, an exact wake-analysis theory for determining force on a body, for both compressible and incompressible flows, was developed by J.Z. Wu and J.M. Wu [9,10] at The University of Tennessee Space Institute. Their theory identifies four lift constituents and four drag constituents, and applies to an arbitrary wake-plane location, and even to the planes cutting through bodies (i.e. upstream of the end of a body), such that the lift and drag contribution upstream of that plane can be determined. Moreover, for incompressible flows, only the velocity field on multi wake planes is needed to apply this theory.

The purpose of this thesis is to apply the incompressible version of Wu and Wu wake-analysis theory using near-wake plane data behind a delta wing in a low subsonic flow, obtained recently from NASA Langley Research Center, and to analyze the results. Also, potential problems of using this theory to a wind-tunnel data need to be identified, so that the theory can be further improved.

Chapter II presents background of the wake-analysis theory used, its assumptions, a brief derivation, and physical interpretation of lift and drag constituents in incompressible formulas.

Chapter III presents information about the wind tunnel in which the data was

acquired, geometry of the model used, flow conditions and a discussion of the data obtained.

Chapter IV describes the application of Wu and Wu wake-analysis theory to the data obtained, the approach for computing the force coefficients, validity of the assumptions, methodology for handling the numerical differentiation and integration, and the treatment of data.

Chapter V presents the results obtained, a comparison of the experimental force coefficient to the measured values, a discussion, and the diagnostics made regarding aerodynamic efficiency.

Chapter VI presents conclusions, recommendations and suggestions for future work.

Chapter II

Theoretical Background

This chapter presents background information about the assumptions in Wu and Wu wake-analysis theory, its brief derivation from the control volume consideration, physical interpretation of specific terms in incompressible lift and drag formulas, and corrections made to both incompressible and compressible formulas which were misprinted in [9]. For more information, see Wu and Wu [9-11].

2.1 Assumptions

The Wu and Wu wake-analysis theory assumes:

1. Flow is steady and laminar;
2. Control volume is sufficiently large such that the flow is uniform on its front and side boundaries, and it has reached free-stream conditions there;
3. Viscosity is neglected in the wake;
4. For a compressible flow, perfect gas with constant specific heats.

Under these assumptions, which are common to all theories based on control-volume analysis, the theory is exact and it provides theoretical basis for various wake-plane analysis. It can be applied even to planes cutting into a vehicle, so that the contribution of the part of the vehicle upstream of that plane can be determined. The theory naturally leads to a clear distinction of the lift and drag constituents based on the flow physics, and the main source of the net aerodynamic force is localized in vortical regions, as will be seen later. These are the significant advancements compared to

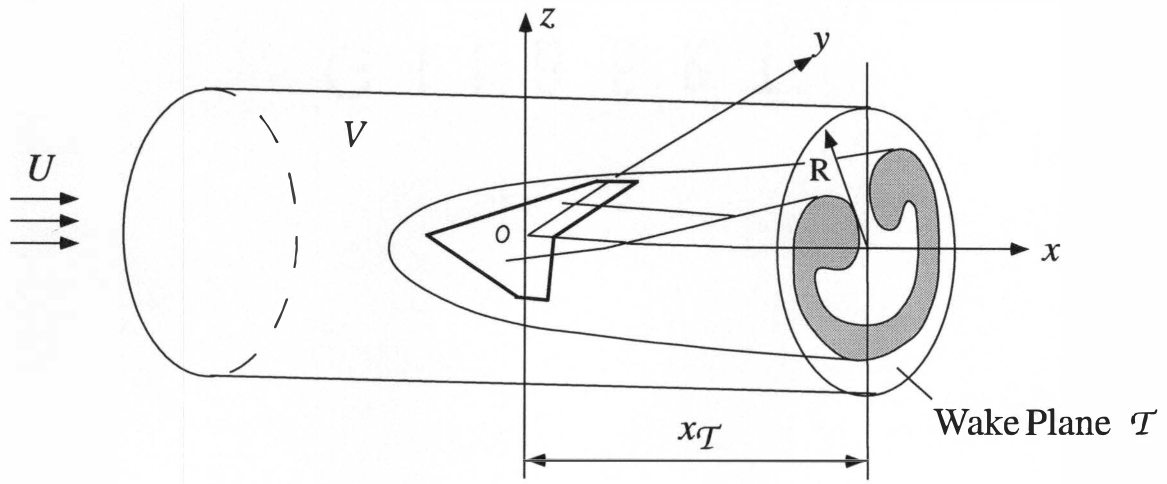

Figure 2.1: Control Volume and the Wake Plane (Reproduced from [9])

the available theories to date.

2.2 Control Volume Analysis

Let V be a control volume bounded by an outer boundary, the control surface ∂V, and an inner boundary, the stationary body surface ∂B (see Fig.2.1). Applying the momentum balance to the flow in V and using adherence condition on ∂B, as well as the assumptions 1 and 3 stated in §2.1, one obtains the well-known formula of total force $\boldsymbol{F}$ acted on ∂B:

$$\boldsymbol{F} = -\int_{\partial V} (p\boldsymbol{n} + \rho\boldsymbol{u}\boldsymbol{u}\cdot\boldsymbol{n})dS, \tag{2.1}$$

where $\boldsymbol{n}$ is a unit normal vector pointing out of the control volume ∂V. Mathematically, the wake-analysis theory developed by Wu and Wu amounts to an integration by parts of (2.1). The basic ideal is as follows. Let $\mathcal{F}$ be an arbitrary tensor, and $\circ$ be any admissible product operator. Then on an arbitrary surface S, the following generalized Stokes theorem holds [10]:

$$\int_S (\boldsymbol{n}\times\boldsymbol{\nabla})\circ\mathcal{F} = \oint_{\partial S} \boldsymbol{dl}\circ\mathcal{F} \tag{2.2}$$

where $\boldsymbol{n}$ is the unit normal of S and $\boldsymbol{dl}$ is the line element of ∂S. In particular, if S is closed such that $\partial S = 0$, or if $\mathcal{F}$ is uniform on ∂S, then

$$\int_S (\boldsymbol{n} \times \boldsymbol{\nabla}) \circ \mathcal{F} = 0. \tag{2.3}$$

Therefore, if one can rearrange terms in (2.1), so that some parts of them cancel each other due to (2.3), then the remained parts must be irreducible in the sense that only these parts have the net contribution to the total force. To obtain such an irreducible force formula, one needs a transformation of the integrand in (2.1). First, make an orthogonal decomposition of the integrand in (2.1) into: $\phi \boldsymbol{n} + \boldsymbol{n} \times \boldsymbol{A}$, where $\phi = p + \rho(\boldsymbol{u} \cdot \boldsymbol{n})^2$ and $\boldsymbol{n} \times \boldsymbol{A} = \rho[\boldsymbol{u}\boldsymbol{u} \cdot \boldsymbol{n} - (\boldsymbol{u} \cdot \boldsymbol{n})^2 \boldsymbol{n}]$. Then, using (2.3) (for a closed S), there exist a pair of integral identities [10]:

$$\int_{\partial V} \phi \boldsymbol{n} dS = -\frac{1}{k} \int_{\partial V} \boldsymbol{x} \times (\boldsymbol{n} \times \boldsymbol{\nabla} \phi) dS \tag{2.4}$$

and

$$\int_{\partial V} \boldsymbol{n} \times \boldsymbol{A} dS = -\int_{\partial V} \boldsymbol{x} \times [(\boldsymbol{n} \times \boldsymbol{\nabla}) \cdot (\boldsymbol{A} \times \boldsymbol{n}\boldsymbol{n})] dS, \tag{2.5}$$

where $k = d - 1 = 2$ for three-dimensional flow. Now (2.1) can be recast in terms of ϕ and $\boldsymbol{A}$. Finally, because ϕ and $\boldsymbol{A} \times \boldsymbol{n}$ are under differential operators, and because of assumption 2 stated in §2.1, a contribution to the integrals in (2.4) and (2.5) is only from the wake plane. Therefore, Eq.(2.1) becomes an irreducible wake-plane formula

$$\boldsymbol{F} = \frac{1}{k} \int_{\mathcal{T}} \boldsymbol{x} \times (\boldsymbol{n} \times \boldsymbol{\nabla} \phi) dS + \int_{\mathcal{T}} \boldsymbol{x} \times [(\boldsymbol{n} \times \boldsymbol{\nabla}) \cdot (\boldsymbol{A} \times \boldsymbol{n}\boldsymbol{n})] dS, \tag{2.6}$$

where $\mathcal{T}$ is a wake plane of which the location $x_{\mathcal{T}}$ can be arbitrary (see Fig.2.1). If one chooses a rectangular coordinate system on the wake plane, such that $\boldsymbol{n} = \boldsymbol{\imath}$ is a unit vector along positive x–axis, $\boldsymbol{x} = (x, y, z)$ is a position vector with an arbitrary origin, and $\boldsymbol{u} = (u, v, w)$ is the velocity field, then $\phi = p + \rho u^2$ and $\boldsymbol{A} \times \boldsymbol{n} =$ - ρu $(v\boldsymbol{\jmath} + w\boldsymbol{k})$. Therefore, the three force components from (2.6) read

$$F_x \;=\; D = \frac{1}{k} \int_{\mathcal{T}} \boldsymbol{x} \cdot \boldsymbol{\nabla}_\pi (p + \rho u^2) dS, \tag{2.7}$$

$$F_y = -\int_{\mathcal{T}} z\left[\frac{\partial}{\partial y}(\rho u w) - \frac{\partial}{\partial z}(\rho u v)\right] dS, \tag{2.8}$$

$$F_z = L = \int_{\mathcal{T}} y\left[\frac{\partial}{\partial y}(\rho u w) - \frac{\partial}{\partial z}(\rho u v)\right] dS, \tag{2.9}$$

where F_x, F_y and F_z are drag, side force and lift, respectively, and operator ∇_π means tangent gradient over $\mathcal{T}$, such that $\boldsymbol{x} \cdot \nabla_\pi = (y\partial/\partial y + z\partial/\partial z)$.

Under the same assumptions, the above equations hold for compressible flows. The derivation of both compressible and incompressible lift and drag formulas are included in the Appendix; their final forms, which are applied to the wind tunnel data, are given below. The key feature of (2.6) or (2.7) - (2.9) is that the net force comes only from regions of the wake plane where the flow-field variables change spatially; therefore, regions of constant flow-field variables in the wake plane do not contribute to the net force and the main source of the net force is localized to the vortical regions, where high velocity and vorticity gradients exist. The physical implication of these localized quantities will be clearly seen below.

2.3 Lift in Terms of Wake-Plane Data

For the lift in an incompressible flow, from (2.9), one can obtain the following form

$$L_{inc} = \int_{\mathcal{T}} \rho y u \omega_x dS - \int_{\mathcal{T}} \rho y (v\omega_y + w\omega_z) dS + \int_{\mathcal{T}} \rho y w^2 \frac{\partial}{\partial x}\left(\frac{v}{w}\right) dS; \tag{2.10}$$

The term $\rho y u \omega_x$ shows the close relation between lift and span-wise moment of stream-wise vorticity; it is the dominating term. The term containing $v\omega_y$ and $w\omega_z$ represents the lift due to the side-wash and down-wash of the wake vortices respectively. The last term represents a correction to lift due to the curvature of the wake vortices, and vanishes in a far-wake plane.

For compressible flows, a correction due to density variations has to be added. The

lift formula then becomes

$$
\begin{aligned}
L_{comp} = L_{inc} \quad &+ \quad \int_{\mathcal{T}} \rho y M_x \left[M_z \frac{\partial}{\partial y} - M_y \frac{\partial}{\partial z} \right] h dS \\
&- \quad \int_{\mathcal{T}} \rho y \gamma T M_x \left[M_z \frac{\partial}{\partial y} - M_y \frac{\partial}{\partial z} \right] s dS,
\end{aligned}
\tag{2.11}
$$

where $M_i = u_i/a$ is a Mach Number in the i^{th}-direction. One can see that an additional thermodynamic variable distribution (ρ or T) in the wake plane is needed in order to evaluate the integrals in (2.11).

2.4 Drag in terms of Wake-Plane Data

Similarly, one can rearrange (2.7) (see the Appendix) and obtain the following result for incompressible drag:

$$
\begin{aligned}
D_{inc} \quad &= \quad \frac{2}{k} \int_{\mathcal{T}} \boldsymbol{x} \cdot \boldsymbol{\nabla}_{\pi} p_0 dS + \frac{1}{k} \int_{\mathcal{T}} \boldsymbol{x} \cdot \boldsymbol{\nabla}_{\pi} p dS \\
&+ \quad \frac{2}{k} \int_{\mathcal{T}} \rho \omega_x (zv - yw) dS + \frac{2}{k} \int_{\mathcal{T}} \rho u \frac{\partial}{\partial x} (\boldsymbol{x} \cdot \boldsymbol{u}_{\pi}) dS;
\end{aligned}
\tag{2.12}
$$

where $\boldsymbol{x} \cdot \boldsymbol{u}_{\pi} = yv + zw$, and $k = d - 1 = 2$ for three-dimensional flow.

The first term of (2.12) can be identified as the loss of mechanical energy due to viscous dissipation in the wake (viscous drag). The second term is pressure drag, which is zero if the pressure distribution on the $\mathcal{T}$-plane is uniform. The third term is induced stream-wise force due to the cross-flow velocity components caused by the wake vortices, while the last term represents an effect due to the stream-wise variation of near-field curvature of the cross-flow velocity components, which disappears in a far-wake plane (i.e. the classical Trefftz Plane).

If one replaces p and p_0 by more general variables h and h_0 respectively and adds a term due to the entropy variations, assuming calorically and thermally perfect gas, one obtains the following compressible drag formula:

$$
D_{comp} \quad = \quad \frac{2}{k} \int_{\mathcal{T}} \rho \omega_x (zv - yw) dS + \frac{2}{k} \int_{\mathcal{T}} \rho u \frac{\partial}{\partial x} (\boldsymbol{x} \cdot \boldsymbol{u}_{\pi}) dS
$$

$$
\begin{aligned}
&+ \quad \frac{2}{k}\int_{\mathcal{T}} \rho \boldsymbol{x} \cdot \boldsymbol{\nabla}_{\pi} h_0 \boldsymbol{d}S \\
&+ \quad \frac{1}{k}\int_{\mathcal{T}} \rho (1 + M_x^2) \boldsymbol{x} \cdot \boldsymbol{\nabla}_{\pi} h \boldsymbol{d}S \\
&- \quad \frac{1}{k}\int_{\mathcal{T}} \rho T (3 + \gamma M_x^2) \boldsymbol{x} \cdot \boldsymbol{\nabla}_{\pi} s \boldsymbol{d}S
\end{aligned} \tag{2.13}
$$

where k, M_x, $\boldsymbol{x} \cdot \boldsymbol{\nabla}_\pi$ and $\boldsymbol{x} \cdot \boldsymbol{u}_\pi$ are the same as above.

Chapter III

Wake Planes and Data

This chapter presents information about the wind tunnel at NASA Langley Research Center, in which the wake-plane data was obtained, the model, and orientation of the wake planes. Because the data was not taken for computational purposes but rather for aid in flow visualization, some shortcomings exist, which are discussed below.

3.1 Wind Tunnel Specifications

The data was acquired in the NASA Langley low speed Basic Aerodynamic Research Tunnel - BART, which has the following specifications [12]:

- Test section 28 in H $\times$ 40 in W $\times$ 10 ft L
- Post model support
- Maximum velocity 185 ft/s - Re/ft of 1.14×10^6
- Turbulence intensities of $0.04\% - 0.08\%$

3.2 Wind Tunnel Model

The model used in the wind tunnel was an uncambered 76° delta wing ($b/c = 1/2$), with a flat top surface, triangular cross section, and dimensions as illustrated in Fig.3.1. The wing was set at the angle of attack $\alpha = 20°$. Its projected area perpendicular to the free stream velocity is 27.7 in^2. The cross-sectional area of the wind

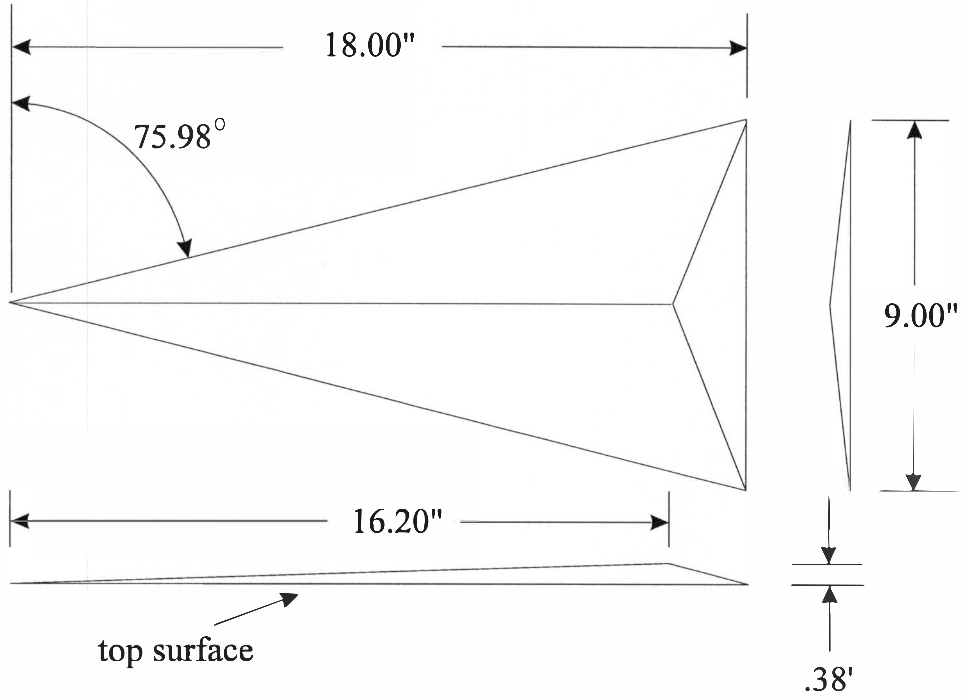

Figure 3.1: Delta Wing Geometry

tunnel is $28 \times 40\ in^2 = 1120\ in^2$, thus the blockage ratio is $(27.7/1120) \approx 2.5\%$. In subsonic wind tunnel flows, the blockage ratio should not exceed 10%; therefore, this model configuration is well within the limits.

3.3 Near-Wake Planes

Three near-wake planes were obtained at $U_\infty \approx 57\ ft/s$ ($M \approx 0.05$ and $Re_c \approx 5 \times 10^5$). The orientation of the wake planes is perpendicular to the upper surface of the delta wing, as illustrated in Fig.3.2, and their locations are $x/c = 0.025$, 0.050 and 0.075 behind the trailing edge, corresponding to $0.45\ in$, $0.90\ in$ and $1.35\ in$, respectively. Because of the time-consuming data-acquisition technique and the symmetry of the flow with respect to (x, z) plane, only one half of the (y, z) plane was collected.

Data was acquired by a five-hole hemispherical probe ($1/8\ in$ diameter), which can simultaneously measure average values of all three velocity components, as well as

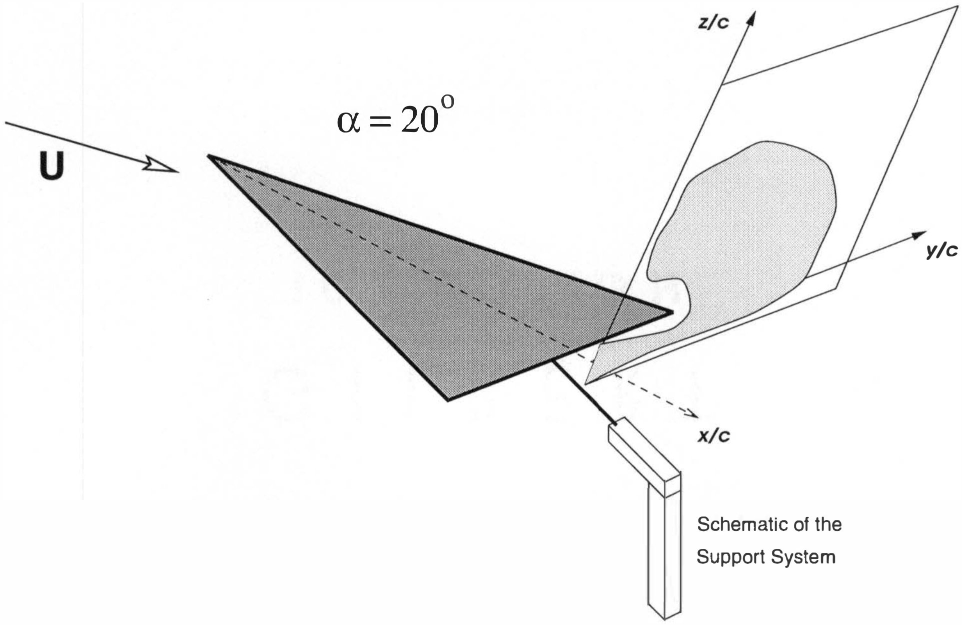

Figure 3.2: Orientation and Location of a Single Wake Plane

static pressure and total pressure. The average time for acquiring a single data point was approximately three seconds, and one wake plane consists of approximately $70 \times 50 = 3,500$ points. In the Table 3.1, the following information is summarized for each wake plane: number of points in y and z-directions (J and K respectively), total number of grid points ($J \times K$), and the size of the wake plane given by four coordinates $(y/c)_{min}$, $(y/c)_{max}$, $(z/c)_{min}$ and $(z/c)_{max}$, measured from the center of the trailing edge, as illustrated in Fig.3.2.

Table 3.1: Wake-Plane Data Summary

x/c	J	K	$J \times K$	$(y/c)_{min}$	$(y/c)_{max}$	$(z/c)_{min}$	$(z/c)_{max}$
1.025	67	49	3283	0	0.33	-0.015	0.225
1.050	67	51	3417	0	0.33	-0.015	0.235
1.075	67	54	3618	0	0.33	-0.015	0.250

3.4 Data Content

All three data sets include the following information: x/c, y/c, z/c, U_∞, u/U_∞, v/U_∞, w/U_∞, C_{p_0}, C_p and a number *iblk* (see below) at each grid point, where

1. x/c is the location of the wake plane, measured axially from the apex of the delta wing;
2. y/c and z/c are the coordinates in span-wise and normal directions to the delta wing respectively (with the origin at the center of the trailing edge) over a rectangular mesh $\Delta y/c \times \Delta z/c = 0.005 \times 0.005$, $(0.09in \times 0.09in)$;
3. U_∞ is the free-stream velocity at the time when the given grid point was measured;
4. u/U_∞, v/U_∞ and w/U_∞ are non-dimensional velocity components in x, y, z directions respectively;
5. $C_{p_0} = (p_0 - p_\infty)/(\frac{1}{2}\rho U_\infty^2)$ is the total pressure coefficient;
6. $C_p = (p - p_\infty)/(\frac{1}{2}\rho U_\infty^2)$ is the static pressure coefficient; and
7. *iblk* is 0.0 for a bad data point which should be discarded, and 1.0 otherwise.

There were three bad points in the data at $x/c = 1.025$, three bad points in the data at $x/c = 1.050$, and no bad points in the data at $x/c = 1.075$. However, the data at the $x/c = 1.025$ location contained four points with negative stream-wise velocity components. Because hemispherical five-hole probes are very inaccurate in measuring negative stream-wise velocity components, this data was treated as bad data as well. The time needed for data acquisition of a single wake plane was several hours, during which the free-stream velocity drifted. Because U_∞ is known at each time when a

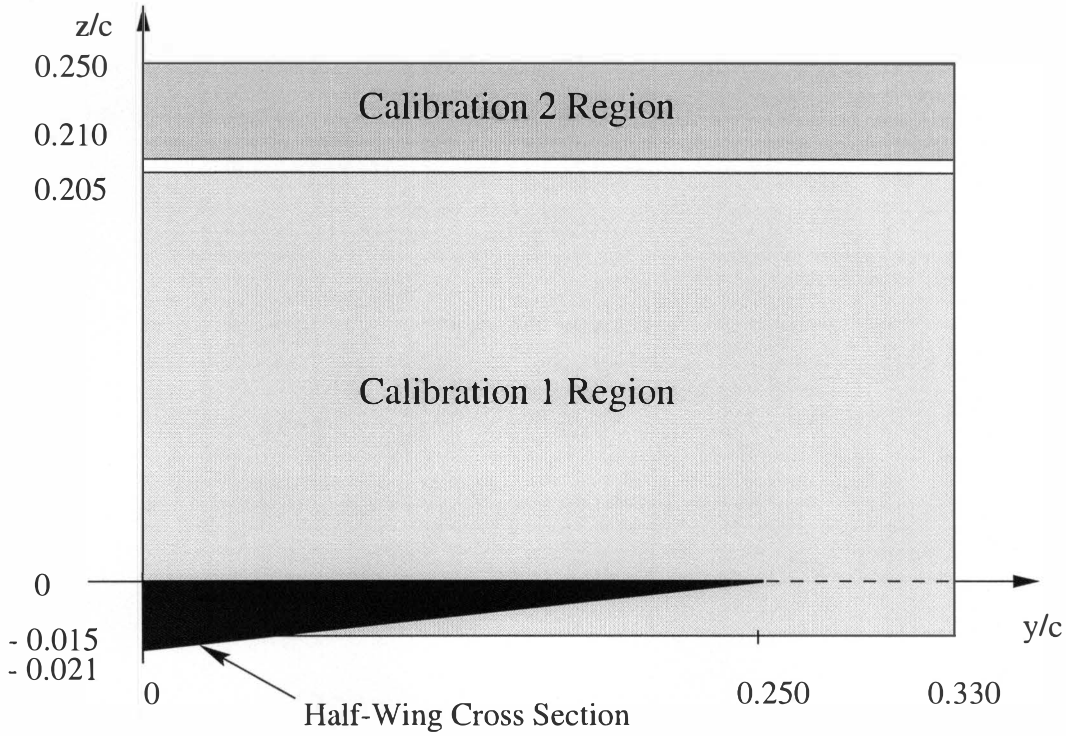

Figure 3.3: Schematic of Calibration Regions

grid point data was acquired, the drift of the free-stream velocity can be computed by

$$U'_{\%} = \frac{U_{max} - U_{min}}{U_{max}} \times 100[\%],$$

where U_{max} and U_{min} are maximum and minimum free-stream velocity values measured at a single wake plane. The maximum detected drift was 3.61% at the wake-plane with $x/c = 1.075$ location. This drift reflects the unsteadiness of the free-stream velocity in the wind tunnel.

Sometimes, the probe used for measurement has to be pitched and yawed, and then re-calibrated. This occured in our wake-plane sets, when the data was acquired in the upper part of the wake plane, for $z/c \geq 0.210$, as illustrated in Fig.3.3. Then, at the line $z/c = 0.210$, which is a region of nearly uniform flow, a jump in all variables (C_{p_0}, C_p, u/U_∞, v/U_∞ and w/U_∞) occured. For illustration, C_{p_0} is plotted in Fig.3.4

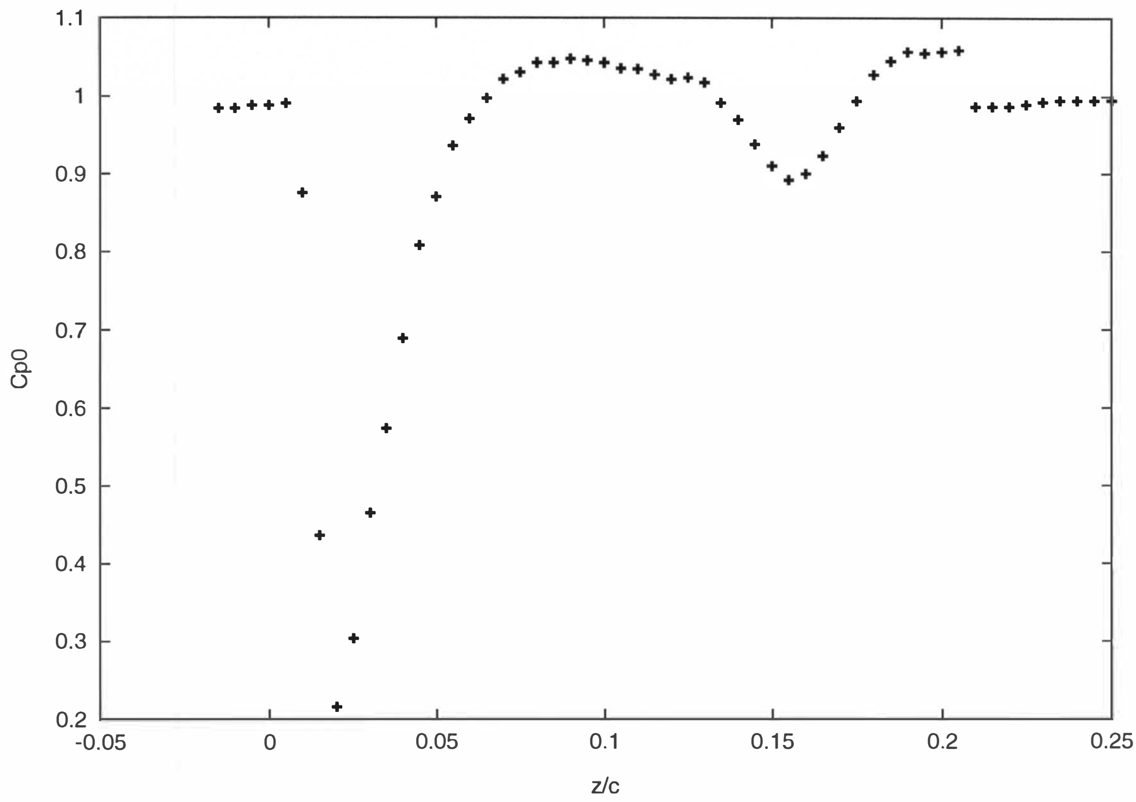

Figure 3.4: Total Pressure Coefficient, C_{p_0}, along z/c-line, at y/c=0.25

along a line parallel to the z-axis at $y/c = 0.25$.

The original non-dimensional velocity, static pressure coefficient and total pressure coefficient distribution, for the wake-plane location $x/c = 1.075$, are plotted in Figures 3.5, 3.6 and 3.7, respectively. The center and the end of the trailing edge in these figures are located at $(y/c, z/c) = (0, 0)$, and $(y/c, z/c) = (0.25, 0)$, respectively. The wake planes at $x/c = 1.050$ and 1.025 have very similar characteristics, and the force coefficients along the span for all wake planes are compared in the results.

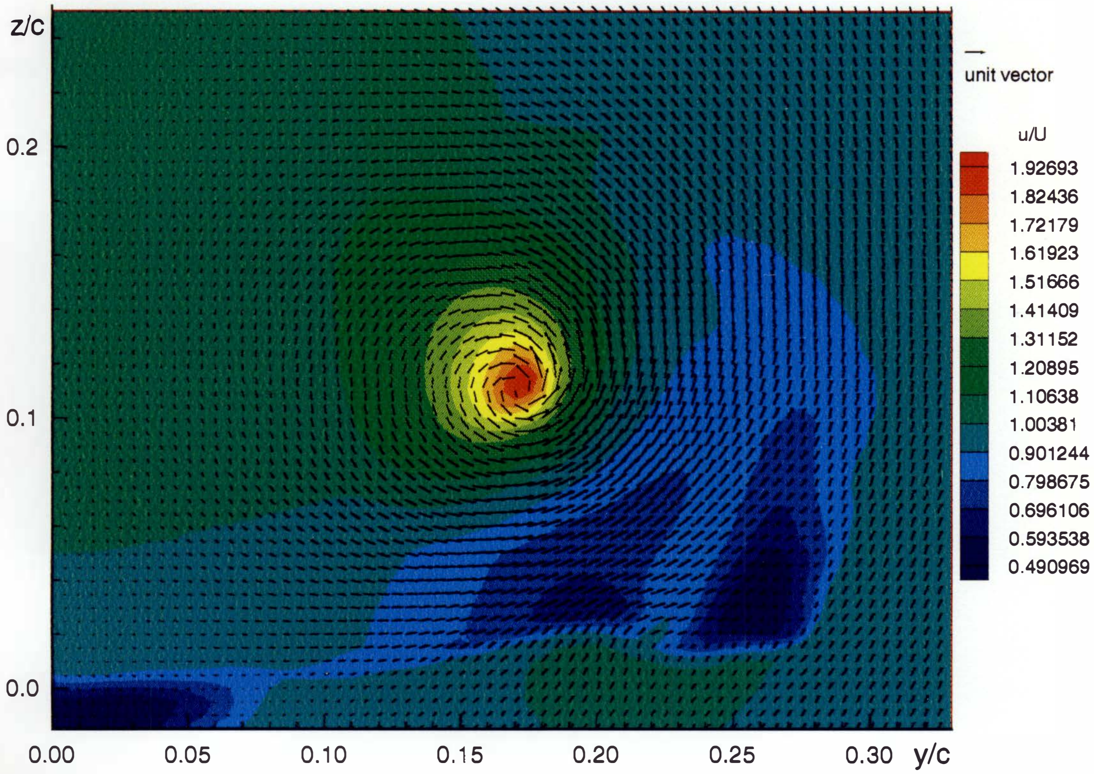

Figure 3.5: Non-dimensional Velocity Field, $\bar{\boldsymbol{u}}$, $x/c = 1.075$.

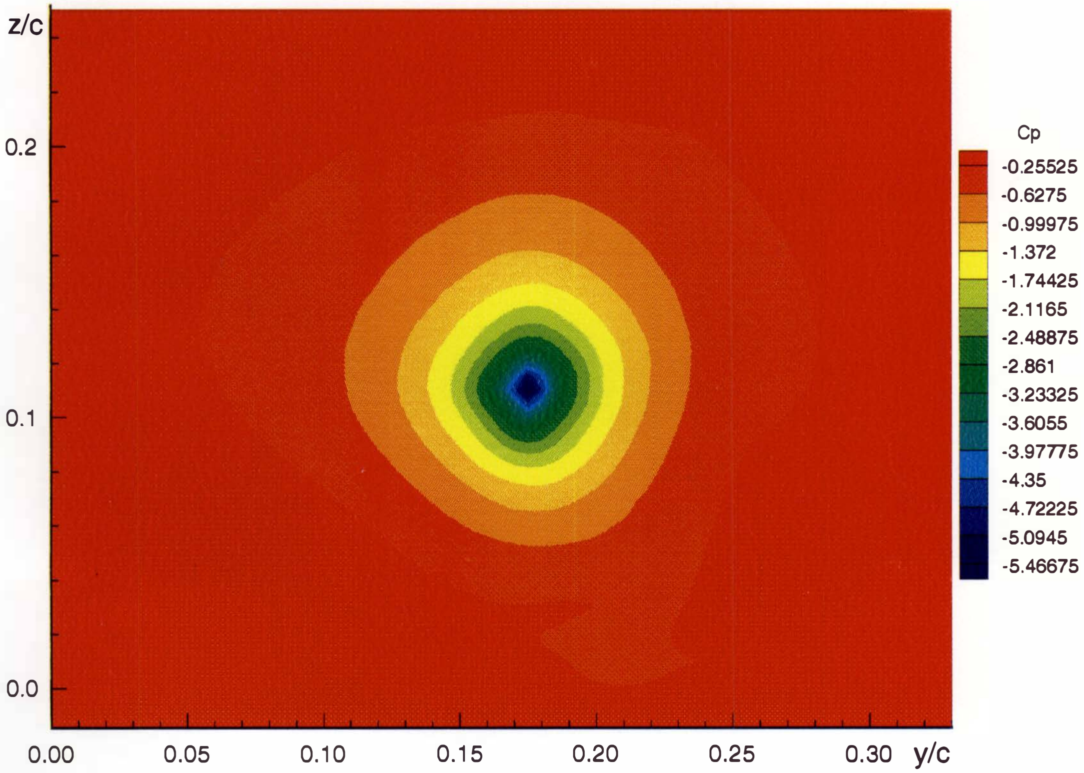

Figure 3.6: Static Pressure Coefficient, C_p, $x/c = 1.075$.

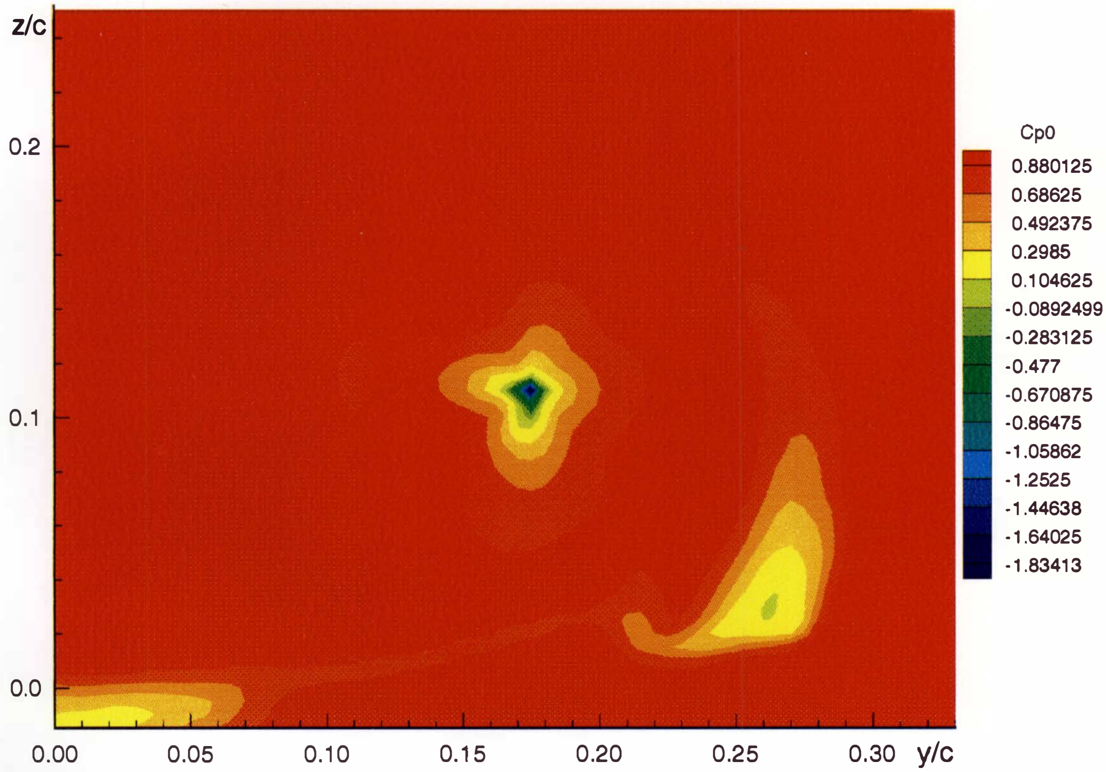

Figure 3.7: Total Pressure Coefficient, C_{p_0}, $x/c = 1.075$.

Chapter IV

Data Processing and Analysis

This chapter describes the application of the Wu and Wu wake-analysis theory to the wake-plane data presented in §3.3 and §3.4, the verification of the assumptions stated in §2.1, the non-dimensional computation of the force coefficients, the handling of numerical differentiation and integration, the treatment of bad data, and a mesh refinement technique.

4.1 Application of the Theory

The wake plane, in Chapter II, was considered to be perpendicular to the free stream velocity; therefore, by orthogonal decomposition of a vector perpendicular and parallel to the wake plane, one may obtain force components perpendicular and parallel to the free stream velocity – drag, side force, and lift. However, the wake-plane data described in §3.3 is in the plane perpendicular to the upper surface of the wing and one might choose a control volume, as illustrated in Fig.4.1. In this case, the orthogonal decomposition of a vector, perpendicular and parallel to the wake plane, leads to the force components perpendicular and parallel to the upper surface of the delta wing –

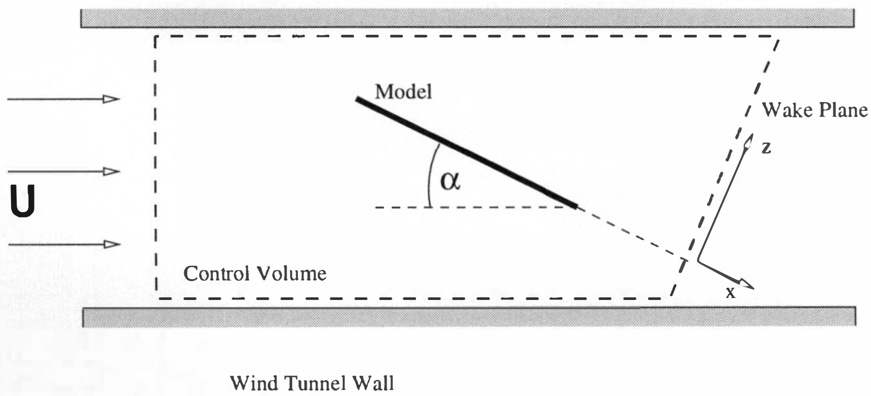

Figure 4.1: Control Volume and the Wake Plane in the Wind Tunnel

axial, normal and side forces. Therefore, all lift and drag constituents given in (2.10) and (2.12) now apply to the constituents of normal and axial forces, respectively. Lift and drag, then, can be computed by a simple transformation

$$\begin{aligned} L &= F_N \cos\alpha - F_A \sin\alpha, \\ D &= F_N \sin\alpha + F_A \cos\alpha, \end{aligned}$$

where α is the angle of attack, and F_N and F_A are the normal and axial forces, respectively. By adapting (2.10), it can be shown that the normal force coefficient is

$$C_{F_N} = \frac{8c}{b}\int_T \bar{y}\left[\bar{u}\Omega_x - \bar{v}\Omega_y - \bar{w}\Omega_z + \bar{w}^2\frac{\partial}{\partial\bar{x}}\left(\frac{\bar{v}}{\bar{w}}\right)\right] d\bar{y}d\bar{z}, \tag{4.1}$$

and similarly, using (2.12), the axial force coefficient becomes

$$\begin{aligned} C_{F_A} &= \frac{4c}{b}\int_T \bar{\boldsymbol{x}}\cdot\bar{\boldsymbol{\nabla}}_\pi C_{p_0} d\bar{y}d\bar{z} + \frac{2c}{b}\int_T \bar{\boldsymbol{x}}\cdot\bar{\boldsymbol{\nabla}}_\pi C_p d\bar{y}d\bar{z} \\ &+ \frac{8c}{b}\int_T \Omega_x(\bar{z}\bar{v} - \bar{y}\bar{w})d\bar{y}d\bar{z} + \frac{8c}{b}\int_T \bar{u}\frac{\partial}{\partial\bar{x}}(\bar{\boldsymbol{x}}\cdot\bar{\boldsymbol{u}}_\pi)d\bar{y}d\bar{z}. \end{aligned} \tag{4.2}$$

Here, spatial coordinates $\bar{\boldsymbol{x}} = (\bar{x},\bar{y},\bar{z})$ are non-dimensionalized by c, velocity $\bar{\boldsymbol{u}} = (\bar{u},\bar{v},\bar{w})$ by U_∞, and vorticity $\boldsymbol{\Omega} = (\Omega_x,\Omega_y,\Omega_z)$ by U_∞/c. The non-dimensional differential area is $d\bar{S} = d\bar{y}d\bar{z} = d(y/c)d(z/c)$. The density cancelled from both equations above, because the forces were non-dimensionalized by dynamic pressure. In order to evaluate (4.1), all vorticity components need to be known; therefore, $\bar{x}$-derivatives of $\bar{v}$ and $\bar{w}$ have to be computed. Because the viscosity in the wake plane is negligible, one can use Euler equations there, obtaining the following results for non-dimensional derivatives.

$$\frac{\partial\bar{v}}{\partial\bar{x}} = -\frac{1}{\bar{u}}\left(\frac{1}{2}\frac{\partial C_p}{\partial\bar{y}} + \bar{v}\frac{\partial\bar{v}}{\partial\bar{y}} + \bar{w}\frac{\partial\bar{v}}{\partial\bar{z}}\right), \tag{4.3}$$

$$\frac{\partial\bar{w}}{\partial\bar{x}} = -\frac{1}{\bar{u}}\left(\frac{1}{2}\frac{\partial C_p}{\partial\bar{z}} + \bar{v}\frac{\partial\bar{w}}{\partial\bar{y}} + \bar{w}\frac{\partial\bar{w}}{\partial\bar{z}}\right), \tag{4.4}$$

Therefore, all three vorticity components and the terms containing x-derivatives in (4.3) and (4.4) can be evaluated from a single plane.

Because three wake planes located close to each other are available ($\Delta x/c = 0.025$), x-derivatives could also be computed from the three planes. However, since the three sets of data were obtained in different days, and since $\Delta x/c$ is still too large compared to $\Delta y/c$ and $\Delta z/c$, the numerical results of using this technique for x-derivative evaluation is not accurate enough to ensure the incompressible continuity equation ($\nabla \cdot \boldsymbol{u} = 0$) and Crocco's theorem ($\nabla p_0 = \rho \boldsymbol{u} \times \boldsymbol{\omega}$). Therefore, this approach was abandoned.

One can see from (4.3) and (4.4) that the first-order differentiation and two-dimensional integration over the area of the wake plane need to be performed. Methods for approaching these problems are discussed in §4.3 and §4.4.

4.2 Validity of the Assumptions

We now check if the assumptions 1,2 and 3 of §2.1 are fulfilled by the data. Assumption 1, steady flow, is not fully satisfied on this set of data, because the free-stream velocity had varied during the time the data was acquired. Because the maximum variation in the free-stream velocity occured over a long time interval (several hours), this unsteady effect can be assumed negligible. Then, assumption 3, neglecting viscosity in the wake plane, was verified by evaluating the viscous term $\mu \nabla \times \boldsymbol{\omega}$ in the wake plane. This term turned out to be $O(10^{-3})$ smaller than ∇p term; therefore, this assumption is met. In contrast, assumption 2 needs a careful check because of the wind-tunnel wall interference and possible insufficient size of the wake-plane area where the data was acquired. The first part of assumption 2, uniform flow on the front boundary, can not be verified from the given data, because the spatial distribution of the free-stream velocity is not known. However, the second part of assumption 2,

free-stream conditions at the boundary of the wake plane, can be checked. Namely, $|\bar{\boldsymbol{u}}| = \sqrt{\bar{u}^2 + \bar{v}^2 + \bar{w}^2}$ and C_{p_0} should be equal to 1, and C_p should be equal to zero at the closed boundary line of the measured part of the wake plane. To illustrate to what extent these are satisfied, $|\bar{\boldsymbol{u}}|$, C_{p_0} and C_p are plotted along the upper and lower line boundaries of the measured part of the wake plane in Figures 4.2, 4.3 and 4.4, respectively. All three figures are plotted over the same absolute range ($\Delta y = 1.0$), in order to see their relative variations.

Moreover, one can see that computation of the first three constituents of the normal force coefficient in (4.1) is limited only to the rotational part of the wake. Also, the induced axial force and the total pressure term in (4.2) are limited only to the rotational part of the wake. Therefore, the magnitude of the non-dimensional vorticity components Ω_x, Ω_y and Ω_z is plotted in Figures 4.5, 4.6 and 4.7 respectively, in order to verify whether the measured part of wake plane contains the whole vortical region.

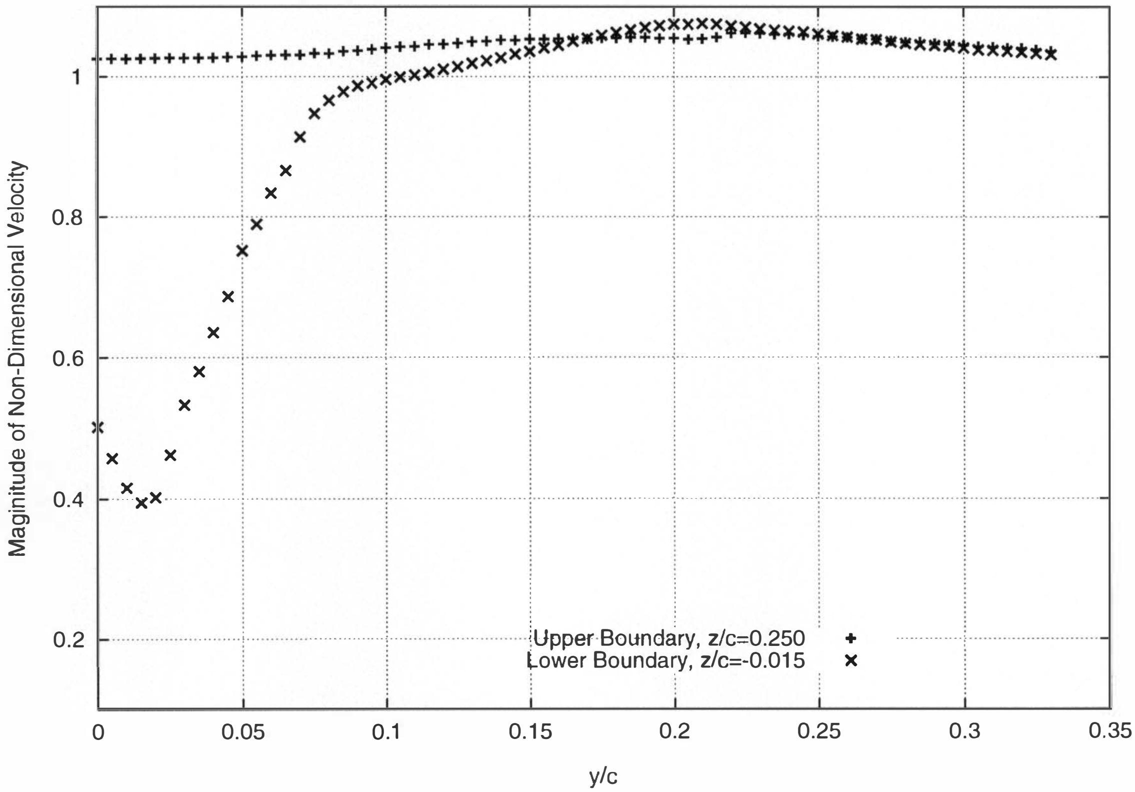

Figure 4.2: Magnitude of the Non-Dimensional Velocity, $\bar{\boldsymbol{u}}$, at the Upper and the Lower Line Boundaries of the Wake Plane, $x/c = 1.075$

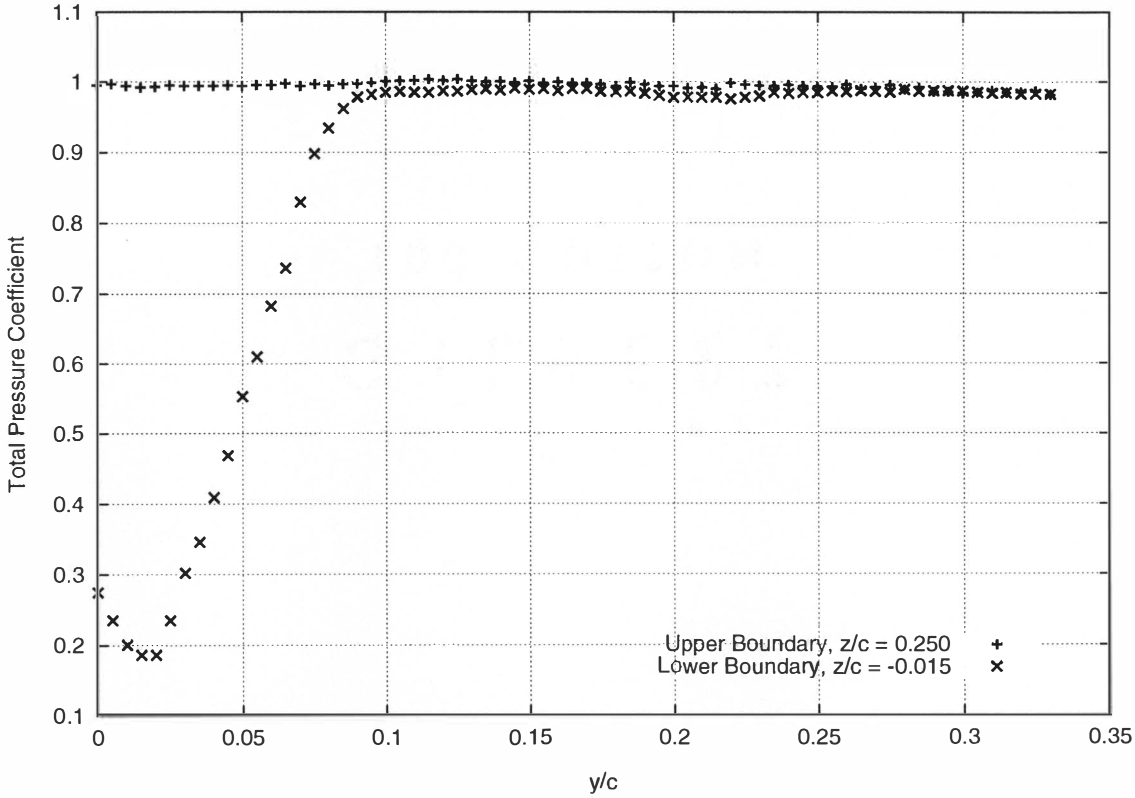

Figure 4.3: Total Pressure Coefficient, C_{p_0}, at the Upper and the Lower Line Boundaries of the Wake Plane, $x/c = 1.075$

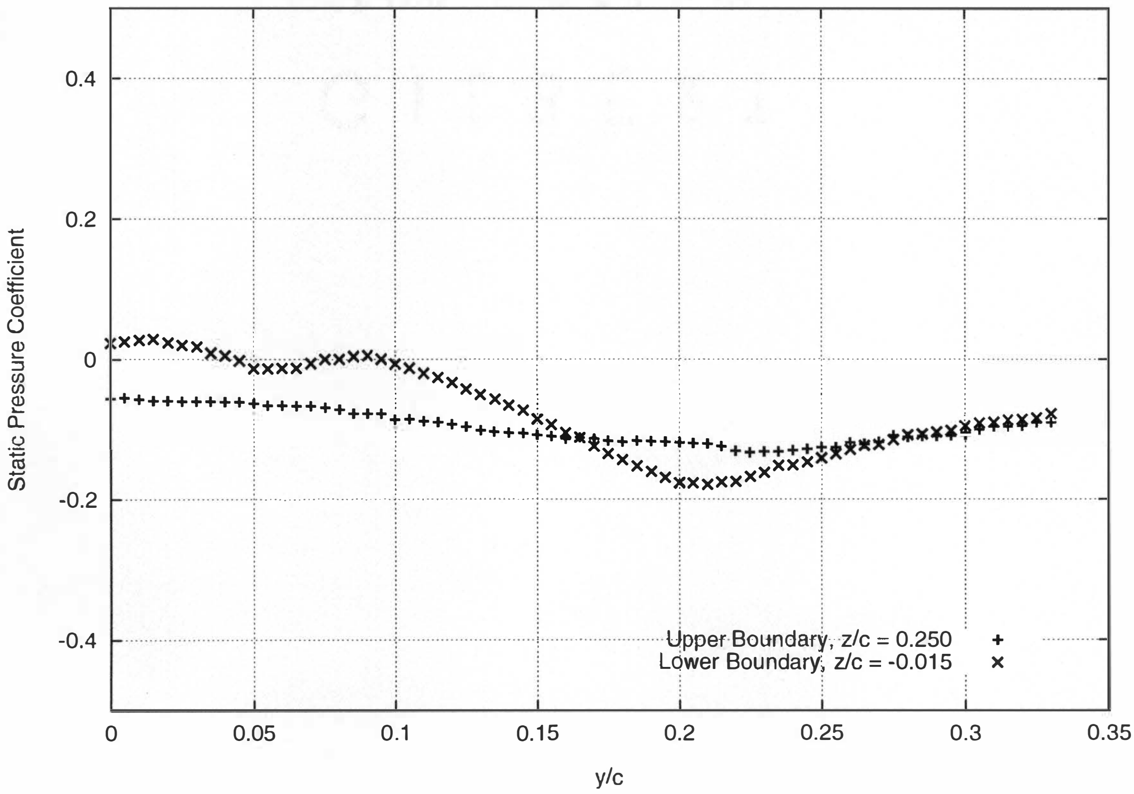

Figure 4.4: Static Pressure Coefficient, C_p, at the Upper and the Lower Line Boundaries of the Wake Plane, $x/c = 1.075$

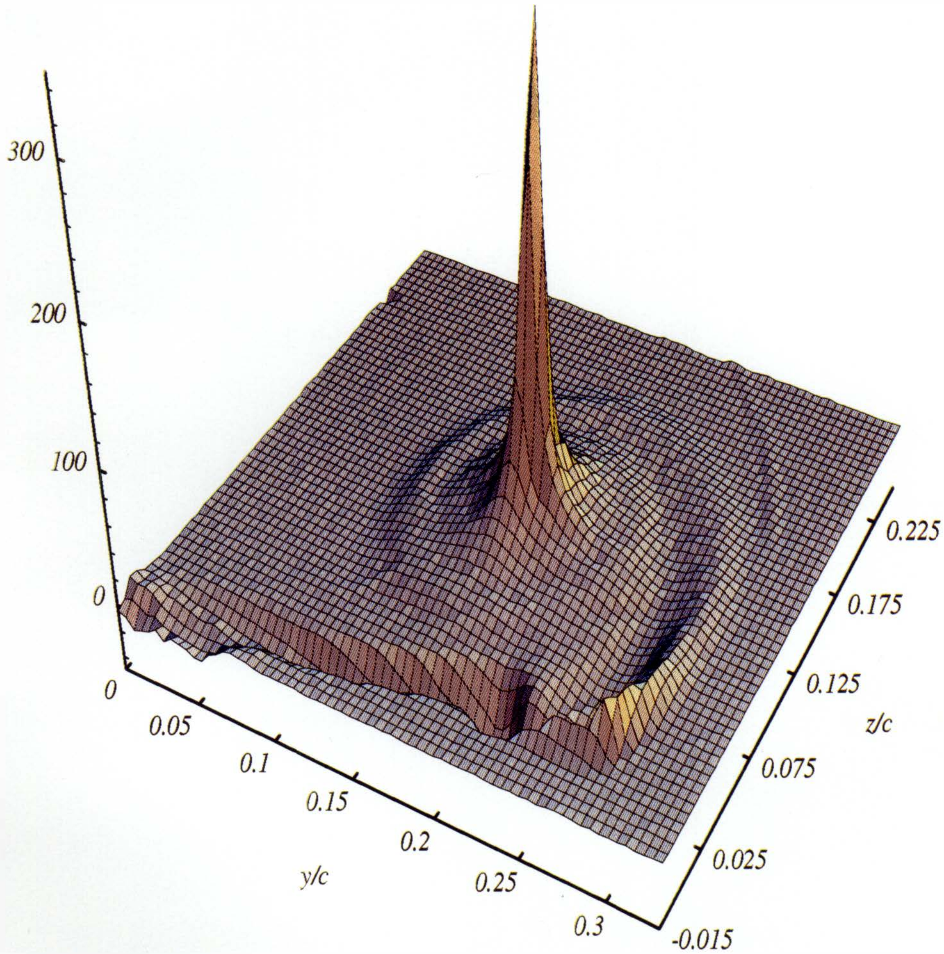

Figure 4.5: Non-Dimensional Axial Vorticity, Ω_x, $x/c = 1.075$

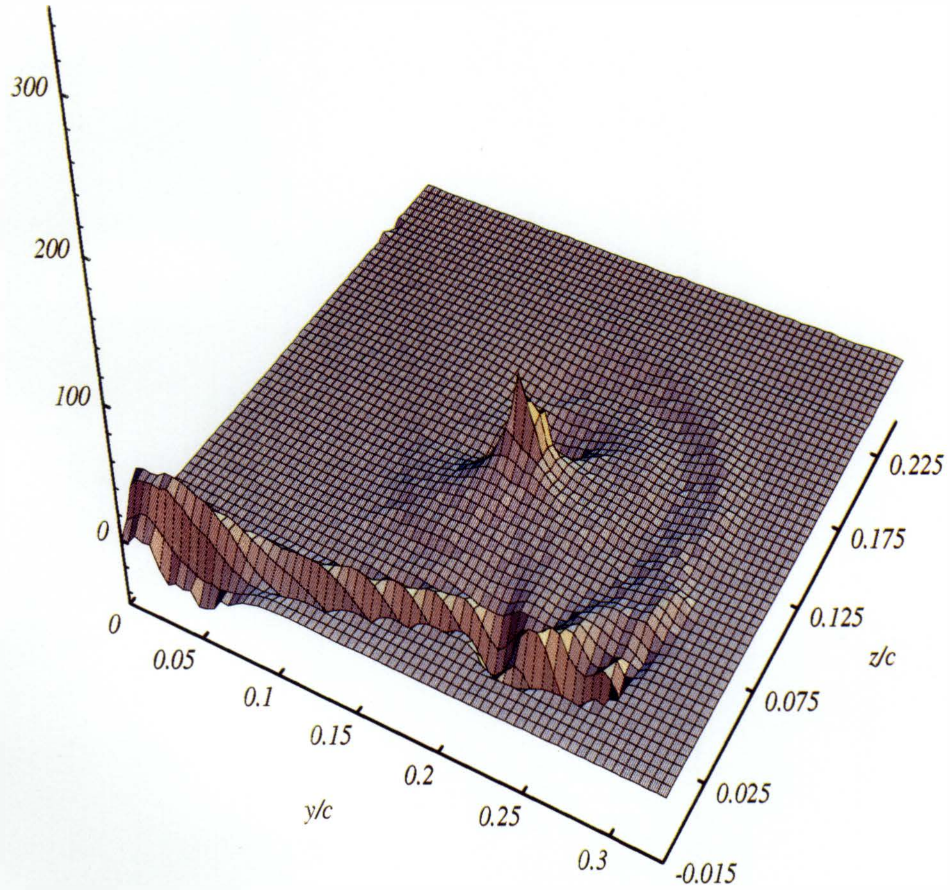

Figure 4.6: Non-dimensional Vorticity Ω_y, $x/c = 1.075$

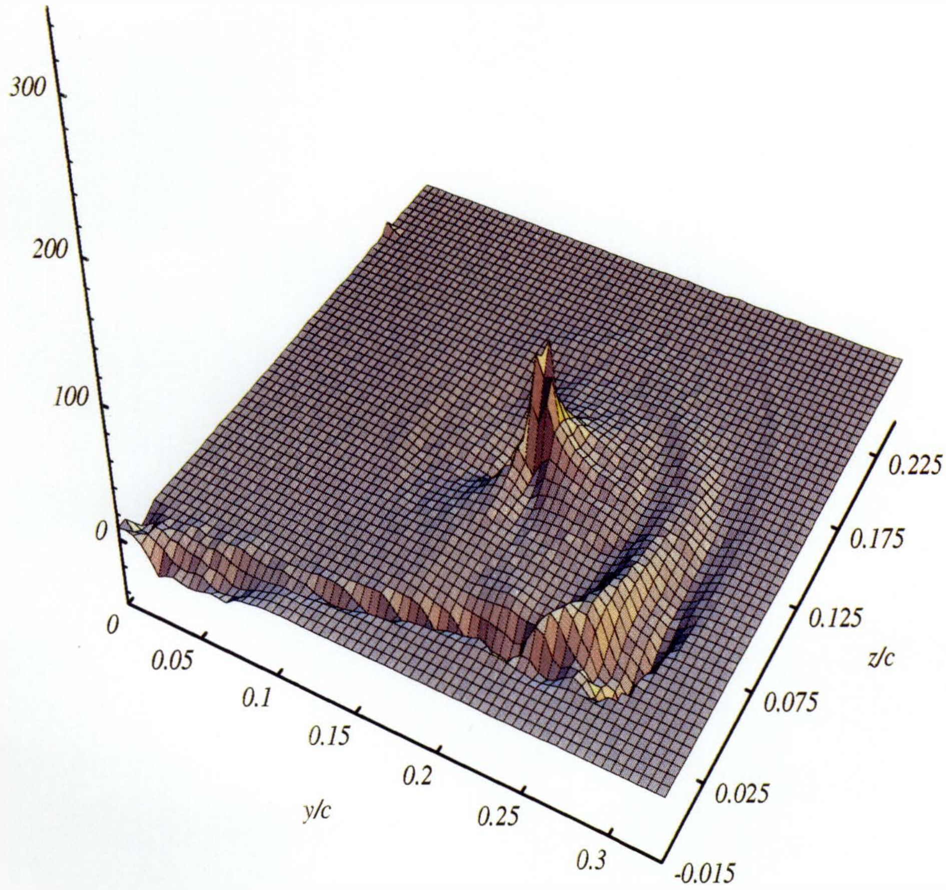

Figure 4.7: Non-dimensional Vorticity Ω_z, $x/c = 1.075$

Now, in Fig. 4.2, $|\bar{\boldsymbol{u}}| \geq 1$ at the whole upper boundary, as well as at the lower boundary of the measured part of the wake plane, except in the region of the model support location. The total pressure coefficient in Fig.4.3 reaches a nearly uniform upstream condition, except the model support location that causes a total pressure loss. The static pressure coefficient in Fig.4.4 is less than zero everywhere, except at the model support location. This is in agreement with Fig.4.2, for if the velocity magnitude exceeds unity, the static pressure coefficient drops below zero. As clearly seen in these three figures, the flow has not reached its uniform upstream conditions at the boundary of the measured part of the wake plane. Therefore, assumption 2 was not met, indicating that measurement should be extended to a larger part of the wake plane, which would contain all of the non-uniformity of the flow. This is illustrated schematically in Fig.4.8.

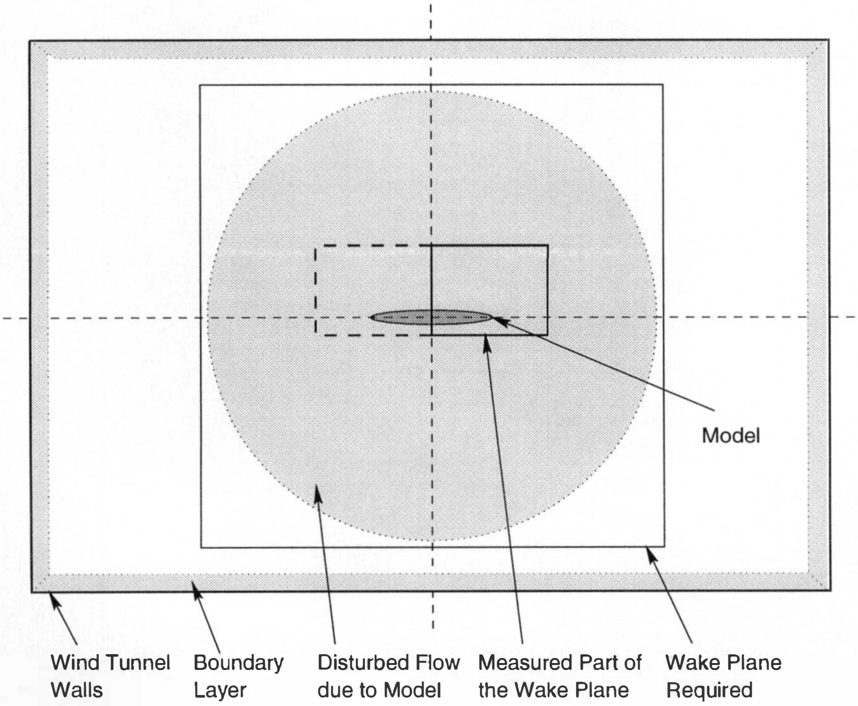

Figure 4.8: Schematic of the Wake Plane Measured and Required for Computation in a Wind Tunnel

Further along, in Figures 4.5, 4.6 and 4.7, a relatively high vortical region can be identified in the vicinity of the model support. In the axial vorticity plot (Fig.4.5), a small vortical region can also be identified at the top boundary of the measured wake plane. The other two vorticity components are nearly zero at the boundary, excluding the model support region.

The above non-uniformities observed on the boundaries of the measured part of the wake plane implies that the simplification from (2.4) and (2.5) to (2.6) must bring some errors. In fact, (2.4) and (2.5) still apply even if these non-uniformities occurs, provided that the data on the side boundaries of the control volume is also available, which is however not the present case. Therefore, we have to tolerate the error caused by these non-uniformities. Essentially, these errors comes from replacing (2.2) by (2.3), i.e. they represent the effect of the right-hand side of (2.2). Note that including a line integral of (2.2) along the boundary of the measured part of the wake plane cannot remove the error. Rather, this boundary line is also that of the (insufficiently large) side boundary surface of the control volume, and a nonzero line integral simply suggests the need for the data on that side boundary.

4.3 Numerical Differentiation

If the measurements are free of errors, then it is appropriate to use the following definition of a derivative

$$\frac{df}{dx} \equiv \lim_{\Delta x \to 0} \frac{\Delta f}{\Delta x}$$

and apply the finite difference approximation. However, the ratio $\Delta f / \Delta x$ proves very sensitive to even the smallest errors if Δx itself becomes too small. One may avoid this by employing the least square method for computing derivatives from empirical data. Basically, this method fits a parabola through k neighboring points from both sides of the point at which the derivative is computed, assuming that the curvature

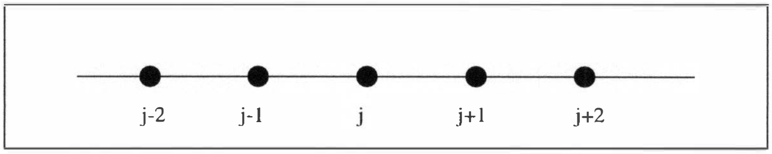

Figure 4.9: Numerical Stencil

of the function does not vary significantly over the points used in the computation. For $k = 2$, a four point stencil, the difference formula for df/dx at an interior point j can be approximated by

$$\frac{df}{dx} \approx \frac{-2f_{j-2} - f_{j-1} + f_{j+1} + 2f_{j+2}}{10h}, \tag{4.5}$$

where h is the grid size, and f is the function evaluated at four different points, as illustrated in Fig.4.9.

On the left and right boundaries the difference formulas have different forms. For more information about this method and about a general formula using k neighboring points, see [13]. For comparison, a five point stencil formula for approximating a derivative of a function was used in order to compare the two results. At an interior point j, it becomes

$$\frac{df}{dx} \approx \frac{f_{j-2} - 8f_{j-1} + 8f_{j+1} - f_{j+2}}{12h}. \tag{4.6}$$

Again, formulas which apply at the right and left boundaries have slightly different forms. The numerical errors regarding the above finite difference formulas are discussed in Chapter V.

4.4 Numerical Integration

For integration, the composite Simpson's rule, adapted for evaluating two-dimensional integrals, was used. For rectangular mesh of size h, the integral of f over the region

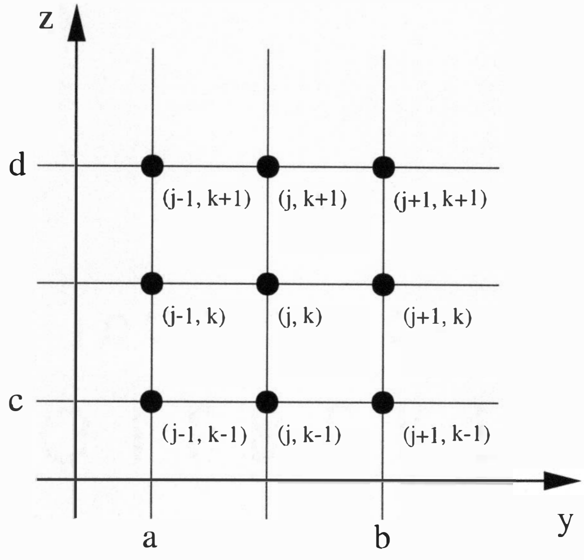

Figure 4.10: Mesh Size for Simpson's Integration Formula

($a \leq y \leq b$, $c \leq z \leq d$), as illustrated in Fig.4.10, is

$$\begin{aligned} \int_c^d \int_a^b f dS &= h^2 \frac{f_{j-1,k-1} + 4f_{j-1,k} + f_{j-1,k+1}}{9} \\ &+ 4\ h^2 \frac{f_{j,k-1} + 4f_{j,k} + f_{j,k+1}}{9} \\ &+ h^2 \frac{f_{j+1,k-1} + 4f_{j+1,k} + f_{j+1,k+1}}{9}. \end{aligned} \tag{4.7}$$

The errors due to numerical integration are discussed in Chapter V.

4.5 Data Correction

If an error occurred during data acquisition, all measured values ($\bar{u}$, $\bar{v}$, $\bar{w}$, C_{p_0} and C_p) were set to zero, and such points were identified by the $iblk$ number, as described in §3.3. Also, if a grid point contained a negative value of $\bar{u}$ (as discussed in §3.3), all data at that grid point was treated as bad data. Because all bad data occurred consecutively along the line parallel to the y/c-axis, the neighboring points along the line parallel to the z/c-axis were used for estimating the values at the bad grid point. A parabolic least-square fit was used to estimate the true values by using two

neighboring points from the point being evaluated. The formula for such a point y_k (see [13]) is

$$\bar{y}_k = y_k - 3\,\frac{y_{k-2} - 4y_{k-1} + 6y_k - 4y_{k+1} + y_{k+2}}{35}, \tag{4.8}$$

where $\bar{y}$ is the new fitted value. The average $(y_{k+1} + y_{k-1})/2$ was the initial value chosen for y_k, in order to get a better prediction than one could expect from using the actual negative or zero values.

The jumps in data, as described in §3.3 and illustrated in Fig.3.4, need to be corrected since they create a steep gradient in all flow variables. By looking at (2.10) and (2.12), one can see that the false contribution to the lift and drag might be significant, if the jumps are not corrected. Observe that in Fig.3.3, the upper region, after re-calibration, is much smaller; furthermore, it is a region of small gradients of the flow-field variables, as can be seen from Figures 3.5, 3.6 and 3.7. Therefore, this smaller region was adjusted to the larger region in order not to alter the dominating part of the data, and also because the products of variables with their gradients are diminishing if the flow variables become nearly constant. Because the difference across the jump slightly varied for each line parallel to the z/c-coordinate, all data in *Calibration 2 Region* (see Fig.3.3) was shifted for each variable, by an average value calculated from all jumps. This average was used in order not to alter the small existing gradients in the direction perpendicular to the jump. After these changes, the data was used for the computation.

4.6 Mesh Refinement

When applying the numerical stencil for derivatives of an empirical function, one assumes that the curvature of the function does not change significantly between the points from which the derivative is computed. If these points are not sufficiently close

together, this assumption might not be valid, and error in the least square fit might be significant. One has to be especially careful in the vortex core region, where the velocity gradients change significantly. In order to minimize the least square error, the mesh was refined and the spline technique [14] was used for interpolating values between two consecutive points. Three different mesh refinements were made, wherein the side of a cell was divided into 2, 4 and 8 smaller segments, thus dividing each grid cell into 4, 16 and 64 smaller cells, respectively. The original mesh over which data was obtained is $\Delta y/c \times \Delta z/c = 0.005 \times 0.005$, corresponding to $0.09\ in \times 0.09\ in$.

Chapter V

Results and Discussion

This chapter summarizes quantitative results obtained from the three data sets; computed force coefficients are compared to the experimental values. A physical interpretation of the span-wise distribution of the force coefficients is made and sources of errors are discussed.

5.1 Quantitative Results and Discussion

Two sets of experimental values for C_L and C_D, by a wind tunnel balance, were obtained from NASA Langley Research Center. The first set was not corrected for the wall interference or model support in the wind tunnel. The coefficients are

$$C_L = 0.744 \text{ and } C_D = 0.314.$$

The second set was corrected only for the wind-tunnel-wall interference using the Wall-Pressure Signature Correction Method described in [12,15]. These values are

$$C_L = 0.690 \text{ and } C_D = 0.243.$$

Values corrected for the support interference has not been obtained. From the above values, it is apparent that the wind tunnel walls had a significant influence on the flow. The correction made to the lift coefficient is $(0.744 - 0.690)/0.744 \approx 7.3\%$, and to the drag coefficient $(0.314 - 0.243)/0.314 \approx 22.6\%$. Since the blockage ratio was only 2.5% and the flow was low subsonic ($U_\infty \approx 57\ ft/s$, $M \approx 0.05$), it is not well understood why the wall interference had such a large effect on the flow. Because all interferences were reflected in the measured wake data, computed values

should be compared to the uncorrected experimental values. The final results of C_L and C_D computed from the three wake planes are summarized in Table 5.1. Three refinements of the original grid were made by dividing the cell into 4, 16 and finally 64 smaller cells, in order to see the grid size effect on the final results. Two derivative techniques were used, as described in §4.3, to compare the consistency of the results after different refinements were made.

Observe from Table 5.1 that the computed drag coefficients are larger than the experimental uncorrected value of 0.314, and that the computed lift coefficients are far below the uncorrected value of 0.744. Since the assumptions of the wake-plane theory are not completely met (mainly the flow is non-uniform of the side walls of the control volume, set by the wake plane), additional correction terms need to be included. However, additional data is needed in order to evaluate these terms. Specifically, data on the side walls of the control volume would be required. In a case flow was not uniform upstream of the model, the upstream velocity distribution would also be required. Because this additional data is not available, the correction terms can not be evaluated.

Further, one can see from Table 5.1 that the results obtained for a single plane using the $5-point$ stencil are almost identical to four decimal places, but values computed by using the stencil for empirical data are much less consistent. This suggests that the original mesh is fine and accurate enough for computing derivatives by the $5-point$ stencil, and that the numerical error introduced is $O(10^{-4})$. Therefore, using the stencil for empirical data might not apply to this data, since large curvature changes exist in the vortex core, and the derivatives are highly smoothed in that region.

Table 5.1: Computed Lift and Drag Coefficients from the Three Wake Planes

x/c location	$n \times n$ refinement	$Numerical$ $Stencil$	$Computed$ C_L	$Computed$ C_D
1.025	2×2	$Parabolic\ Fit$	0.6638	0.3373
1.025	2×2	$5 - point$	0.6637	0.3395
1.025	4×4	$Parabolic\ Fit$	0.6638	0.3389
1.025	4×4	$5 - point$	0.6636	0.3395
1.025	8×8	$Parabolic\ Fit$	0.6637	0.3393
1.025	8×8	$5 - point$	0.6635	0.3396
1.050	2×2	$Parabolic\ Fit$	0.6636	0.3327
1.050	2×2	$5 - point$	0.6627	0.3345
1.050	4×4	$Parabolic\ Fit$	0.6629	0.3340
1.050	4×4	$5 - point$	0.6627	0.3345
1.050	8×8	$Parabolic\ Fit$	0.6629	0.3340
1.050	8×8	$5 - point$	0.6627	0.3345
1.075	2×2	$Parabolic\ Fit$	0.6748	0.3263
1.075	2×2	$5 - point$	0.6740	0.3285
1.075	4×4	$Parabolic\ Fit$	0.6742	0.3279
1.075	4×4	$5 - point$	0.6740	0.3285
1.075	8×8	$Parabolic\ Fit$	0.6740	0.3283
1.075	8×8	$5 - point$	0.6740	0.3285

Tables 5.2, 5.3 and 5.4 summarize the results for the wake-plane locations $x/c = 1.025, 1.050$ and 1.075, respectively. The magnitudes of normal and axial force coefficients are compared in order to see the importance of the terms in (4.1) and (4.2). For illustration, a computation using only the $5 - point$ stencil is tabulated below.

In the following tables, and the plots in the next section, let

$$C_{F_N} = C_{N_{\Omega_x}} + C_{N_{\Omega_y}} + C_{N_{\Omega_z}} + C_{N_{dx}},$$

where

$$\begin{aligned} C_{N_{\Omega_x}} &= \frac{8c}{b} \int_T \bar{y}\bar{u}\Omega_x d\bar{S}, \\ C_{N_{\Omega_y}} &= -\frac{8c}{b} \int_T \bar{y}\bar{v}\Omega_y d\bar{S}, \\ C_{N_{\Omega_z}} &= -\frac{8c}{b} \int_T \bar{y}\bar{w}\Omega_z d\bar{S}, \end{aligned}$$

and

$$C_{N_{dx}} = \frac{8c}{b} \int_T \bar{y}\bar{w}^2 \frac{\partial}{\partial \bar{x}} \left(\frac{\bar{v}}{\bar{w}} \right) d\bar{S}.$$

Similarly, let

$$C_{F_A} = C_{A_{p0}} + C_{A_p} + C_{A_{\Omega_x}} + C_{A_{dx}},$$

where

$$\begin{aligned} C_{A_{p0}} &= \frac{4c}{b} \int_T \bar{\boldsymbol{x}} \cdot \bar{\boldsymbol{\nabla}}_\pi C_{p0} d\bar{S}, \\ C_{A_p} &= \frac{2c}{b} \int_T \bar{\boldsymbol{x}} \cdot \bar{\boldsymbol{\nabla}}_\pi C_p d\bar{S}, \\ C_{A_{\Omega_x}} &= \frac{8c}{b} \int_T \Omega_x (\bar{z}\bar{v} - \bar{y}\bar{w}) d\bar{S}, \end{aligned}$$

and

$$C_{A_{dx}} = \frac{8c}{b} \int_T \bar{u} \frac{\partial}{\partial \bar{x}} (\bar{\boldsymbol{x}} \cdot \bar{\boldsymbol{u}}_\pi) d\bar{S}.$$

Table 5.2: Constituents of Normal and Axial Force Coefficients, x/c=1.025

$Constituents$	$Refinement$ 2×2	$Refinement$ 4×4	$Refinement$ 8×8
$C_{N_{\Omega_x}}$	1.0979	1.0980	1.0980
$C_{N_{\Omega_y}}$	-0.1854	-0.1855	-0.1855
$C_{N_{\Omega_z}}$	-0.2221	-0.2222	-0.2222
$C_{N_{dx}}$	0.0494	0.0494	0.0494
C_{F_N}	0.7397	0.7397	0.7397
$C_{A_{p0}}$	0.0893	0.0893	0.0893
C_{A_p}	0.1603	0.1603	0.1603
$C_{A_{\Omega_x}}$	-0.2813	-0.2813	-0.2813
$C_{A_{dx}}$	0.1239	0.1238	0.1238
C_{F_A}	0.0922	0.0920	0.0920

Table 5.3: Constituents of Normal and Axial Force Coefficients, x/c=1.050

$Constituents$	$Refinement$ 2×2	$Refinement$ 4×4	$Refinement$ 8×8
$C_{N_{\Omega x}}$	1.0839	1.0839	1.0839
$C_{N_{\Omega y}}$	-0.1767	-0.1768	-0.1768
$C_{N_{\Omega z}}$	-0.2225	-0.2225	-0.2225
$C_{N_{dx}}$	0.0525	0.0525	0.0525
C_{F_N}	0.7371	0.7371	0.7371
$C_{A_{p0}}$	0.0925	0.0925	0.0925
C_{A_p}	0.1637	0.1637	0.1637
$C_{A_{\Omega x}}$	-0.2875	-0.2876	-0.2876
$C_{A_{dx}}$	0.1190	0.1190	0.1190
C_{F_A}	0.0876	0.0876	0.0876

Table 5.4: Constituents of Normal and Axial Force Coefficients, x/c=1.075

$Constituents$	$Refinement$ 2×2	$Refinement$ 4×4	$Refinement$ 8×8
$C_{N_{\Omega x}}$	1.0940	1.0940	1.0940
$C_{N_{\Omega y}}$	-0.1686	-0.1686	-0.1687
$C_{N_{\Omega z}}$	-0.2211	-0.2212	-0.2212
$C_{N_{dx}}$	0.0414	0.0415	0.0415
C_{F_N}	0.7457	0.77457	0.7457
$C_{A_{p0}}$	0.0947	0.0948	0.0948
C_{A_p}	0.1774	0.1774	0.1774
$C_{A_{\Omega x}}$	-0.2980	-0.2980	-0.2980
$C_{A_{dx}}$	0.1039	0.1040	0.1040
C_{F_A}	0.0781	0.0781	0.0781

From Tables 5.2, 5.3 and 5.4, one can see that the dominant term for the normal force coefficient is the one containing the product of the axial velocity and the axial vorticity. This is not surprising, since the axial velocity is larger in the wake than the cross-flow velocities, and the axial vorticity is always the dominating component, especially in flows around delta wings. The two other vorticity terms represent penalty to normal force, and therefore lift, but they create a positive thrust. Their magnitudes are approximately the same. The last term, curvature effect, is the smallest term, as it was expected.

Regarding the axial force constituents, the term containing the axial vorticity component is the largest and most favorable. It creates positive thrust and positive lift on a vehicle. The remaining terms are not favorable, since they create drag and negative lift. The term containing pressure variations is the second largest term, about twice as large as the viscous term. When considering the remaining term, notice that the axial perturbation in the near wakes is quite large; therefore, this term can not be neglected close to a vehicle. However, moving farther downstream, this term would become negligible.

5.2 Physical Interpretation of Results and Discussion

The constituents of the normal and axial forces were described quantitatively in the previous section. In the following figures, they are plotted along the span of the delta wing. Due to integration by parts of the original momentum equation, these plots do not reflect span-wise load distribution. However, they indicate the contributions to the force components. In Figures 5.1,5.5 and 5.9, the three constituents in the total normal force coefficient (4.1) are plotted along the span for wake-planes located at $x/c = 1.025$, 1.050 and 1.075 respectively. Similarly, Figures 5.2,5.6 and 5.10 include the four constituents of the total axial force coefficient (4.2) along the wake-plane span located at x/c=1.025, 1.050 and 1.075, respectively. The total normal and axial force coefficient distributions for wake-planes located at $x/c = 1.025$,1.050 and 1.075 are included in Figures 5.3, 5.7 and 5.11, respectively. This is in order to visualize the magnitudes as well as the relative importance of these total force coefficients. Moreover, lift and drag coefficient distributions along the span for wake planes located at x/c=1.025, 1.050 and 1.075 are plotted in Figures 5.4, 5.8 and 5.12, respectively. From these plots, the aerodynamic efficiency (C_L/C_D) can be identified for various span locations. To emphasize again, these plots are not the load distributions along the span, due to integration by parts, but rather the distributions based on the characteristic of the flow. These points are clarified right after the figures. Finally, Figures 5.13 and 5.14 include the evolution of the lift and drag coefficient distributions along the span from the three wake planes.

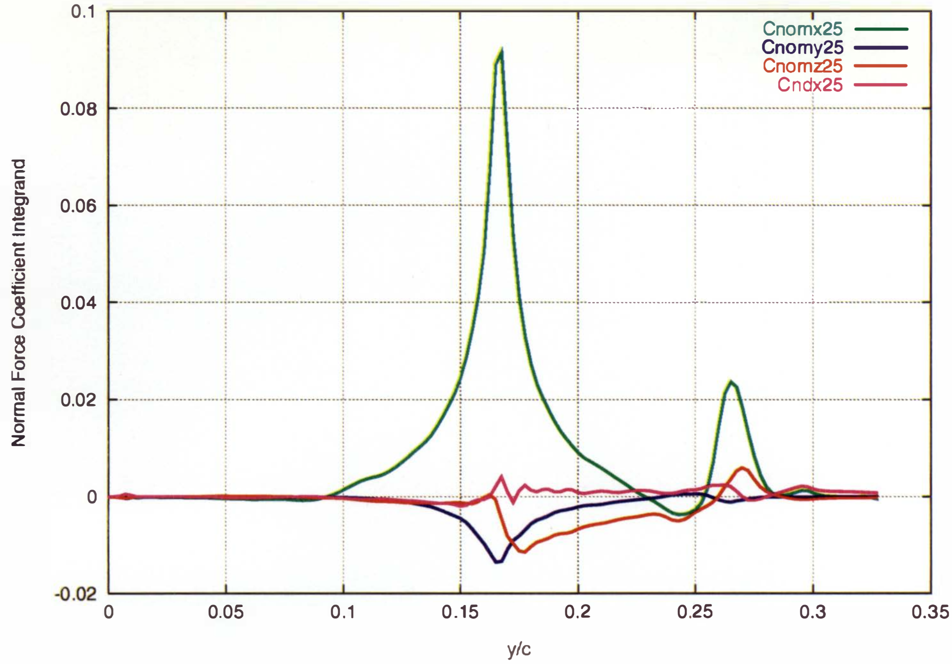

Figure 5.1: Constituents of Normal Force Coefficients, x/c=1.025

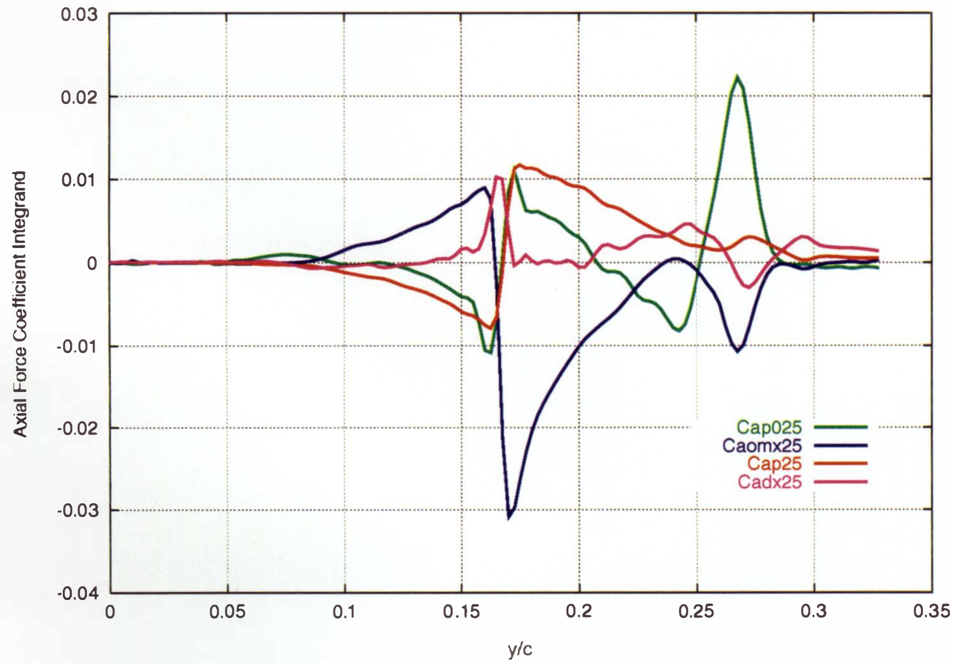

Figure 5.2: Constituents of Axial Force Coefficients, x/c=1.025

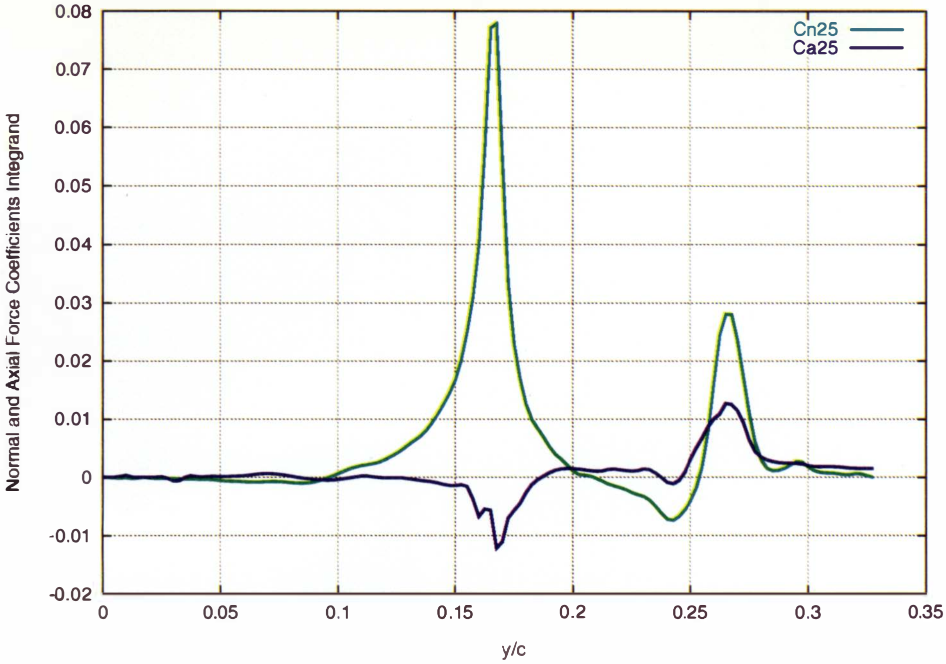

Figure 5.3: Total Normal and Axial Force Coefficients, x/c=1.025

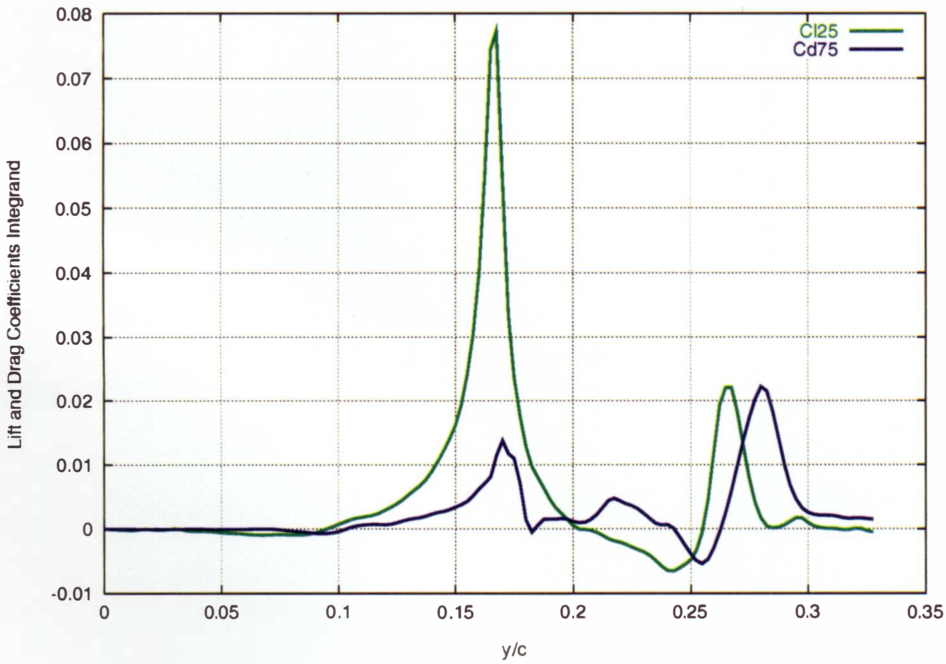

Figure 5.4: Lift and Drag Coefficients, x/c=1.025

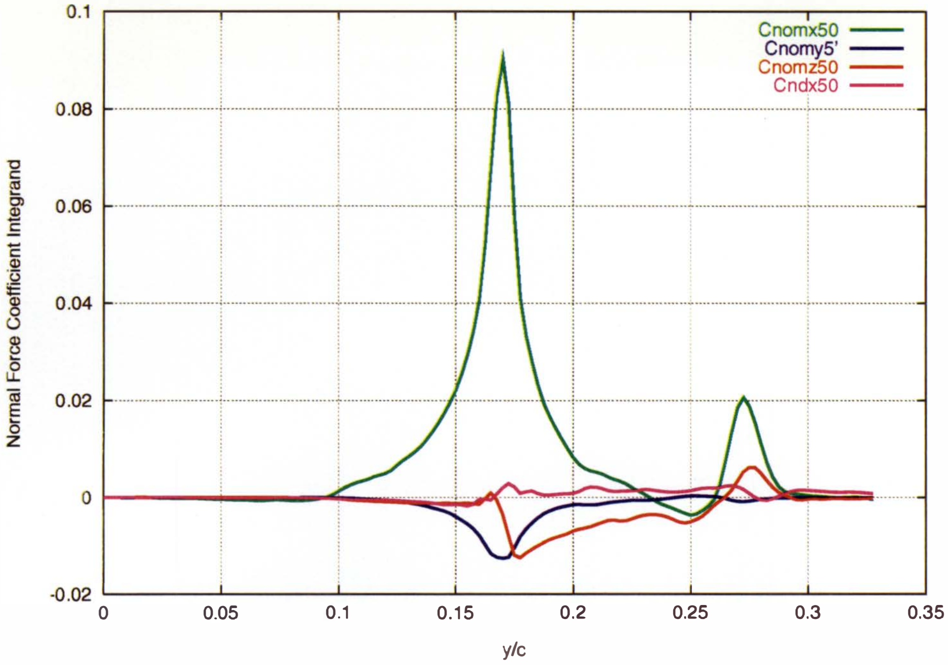

Figure 5.5: Constituents of Normal Force Coefficients, x/c=1.050

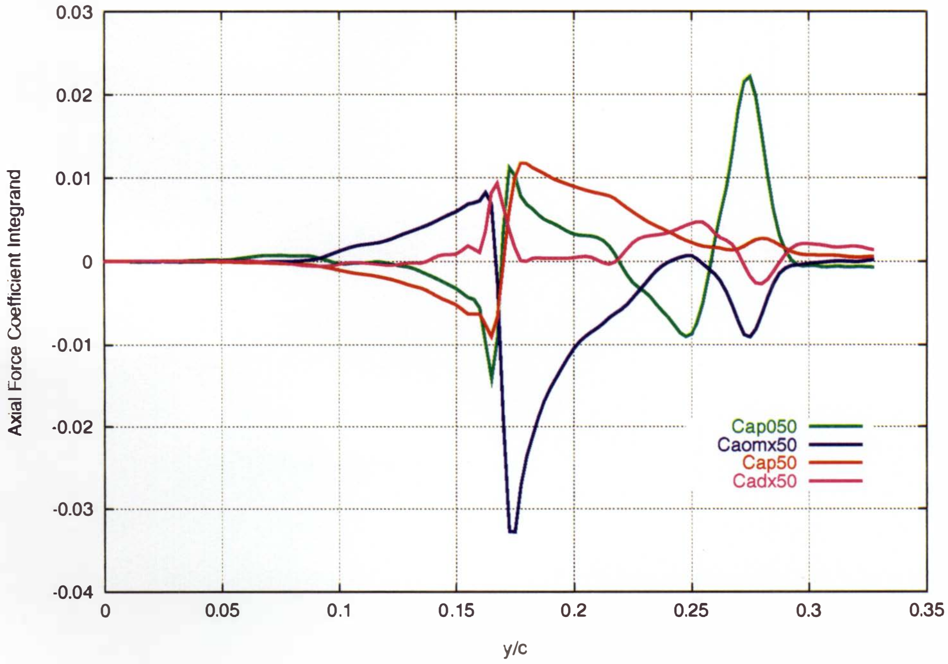

Figure 5.6: Constituents of Axial Force Coefficients, x/c=1.050

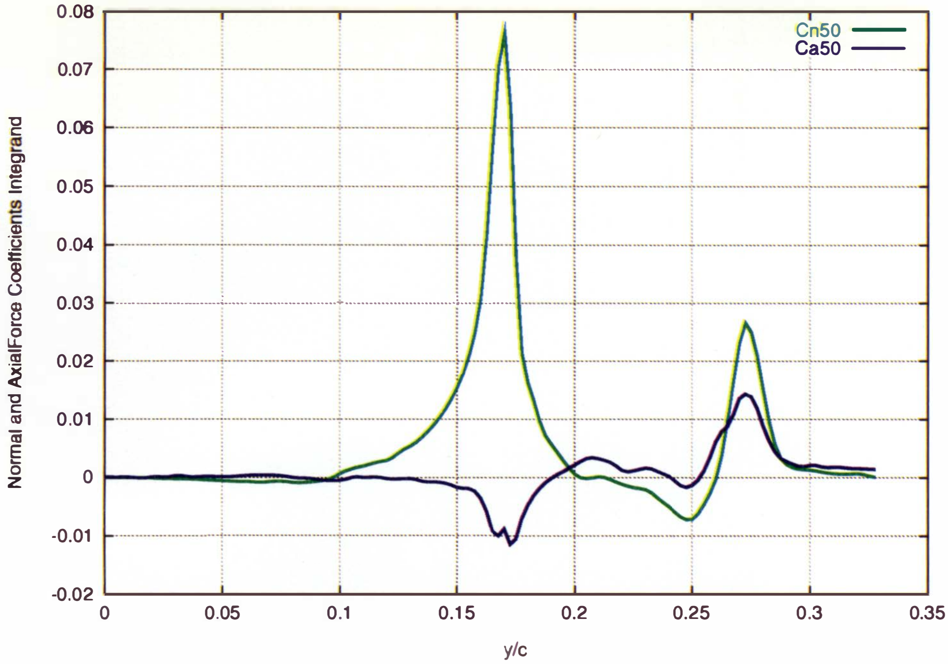

Figure 5.7: Total Normal and Axial Force Coefficients, x/c=1.050

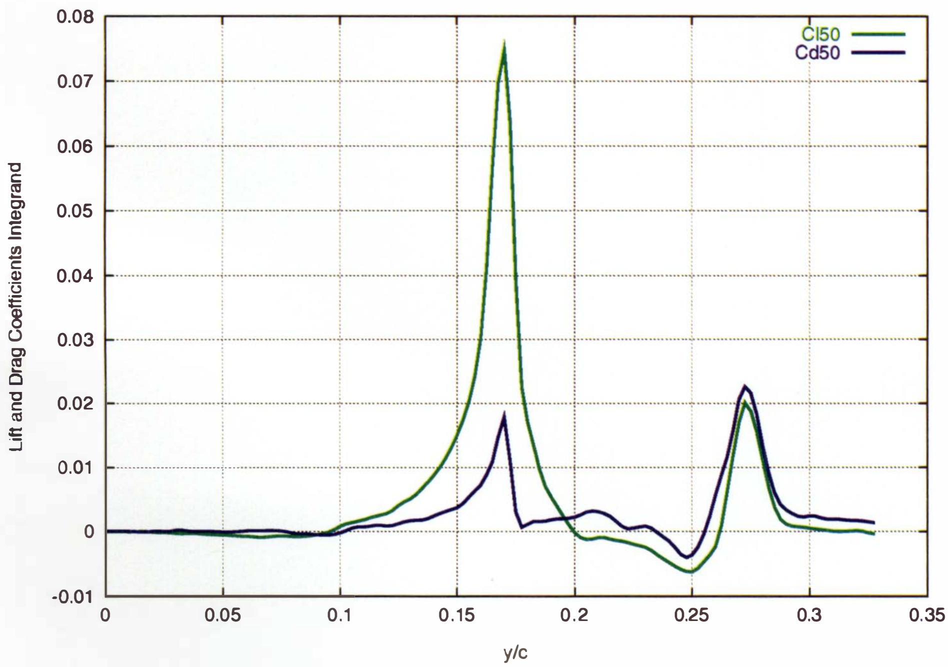

Figure 5.8: Lift and Drag Coefficients, x/c=1.050

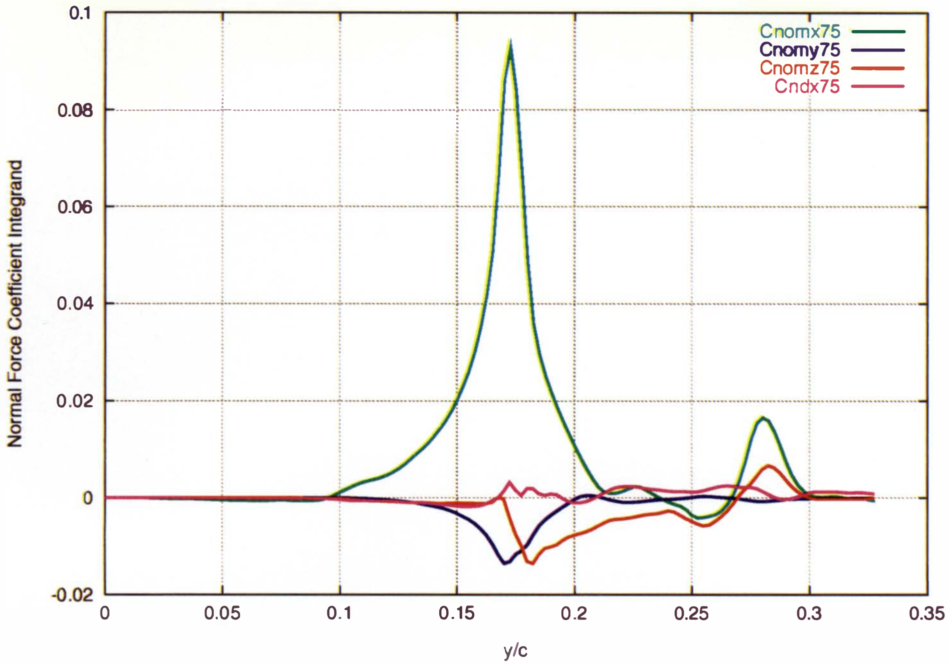

Figure 5.9: Constituents of Normal Force Coefficients, x/c=1.075

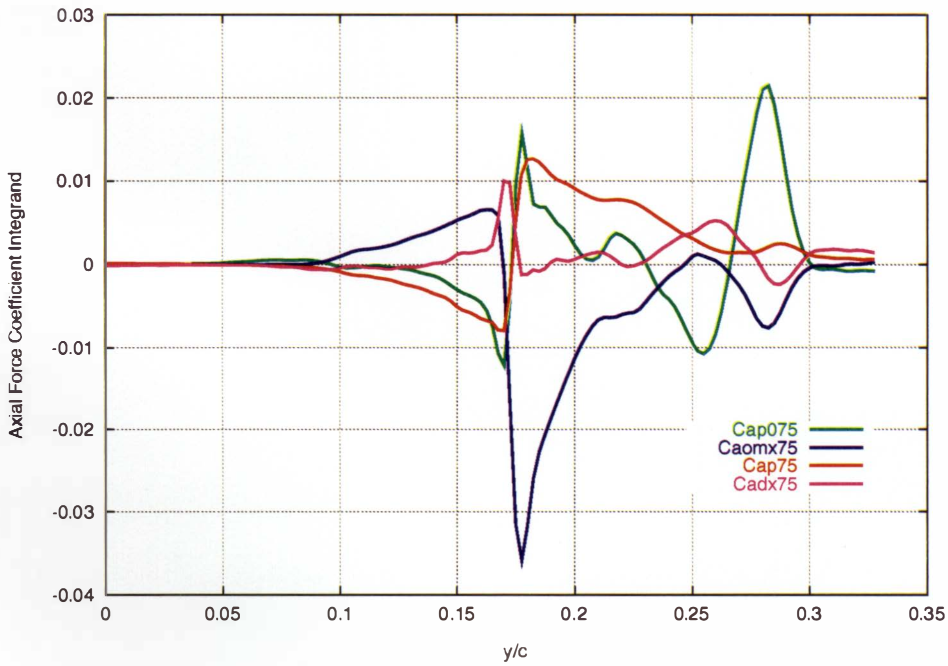

Figure 5.10: Constituents of Axial Force Coefficients, x/c=1.075

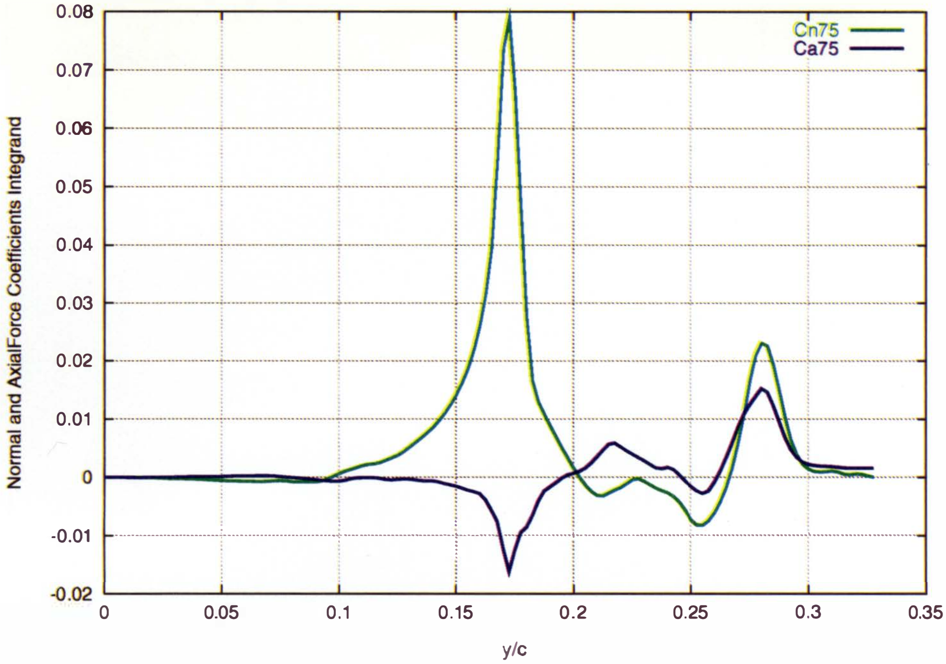

Figure 5.11: Total Normal and Axial Force Coefficients, x/c=1.075

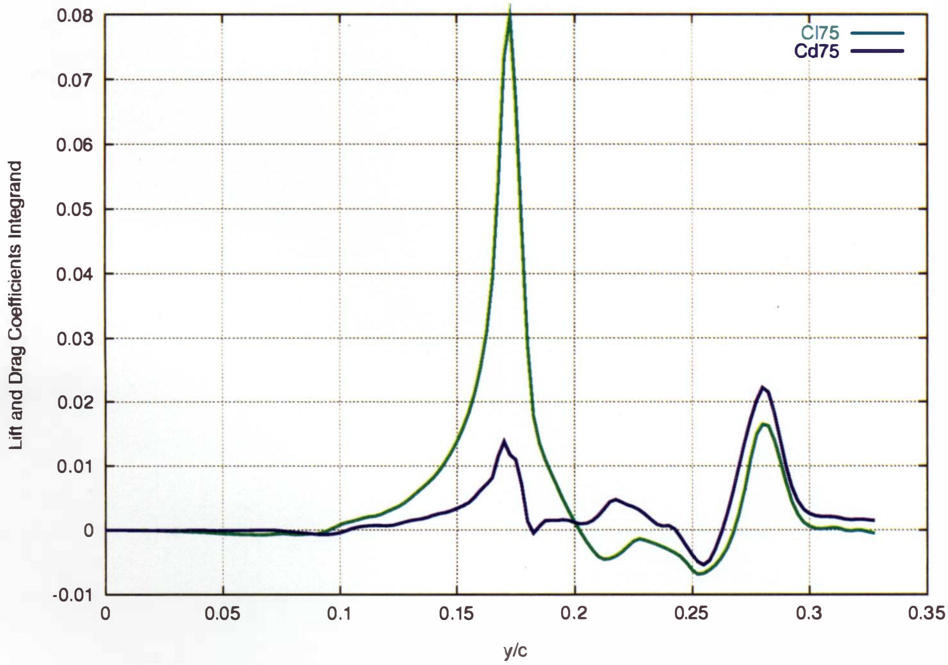

Figure 5.12: Lift and Drag Coefficients, x/c=1.075

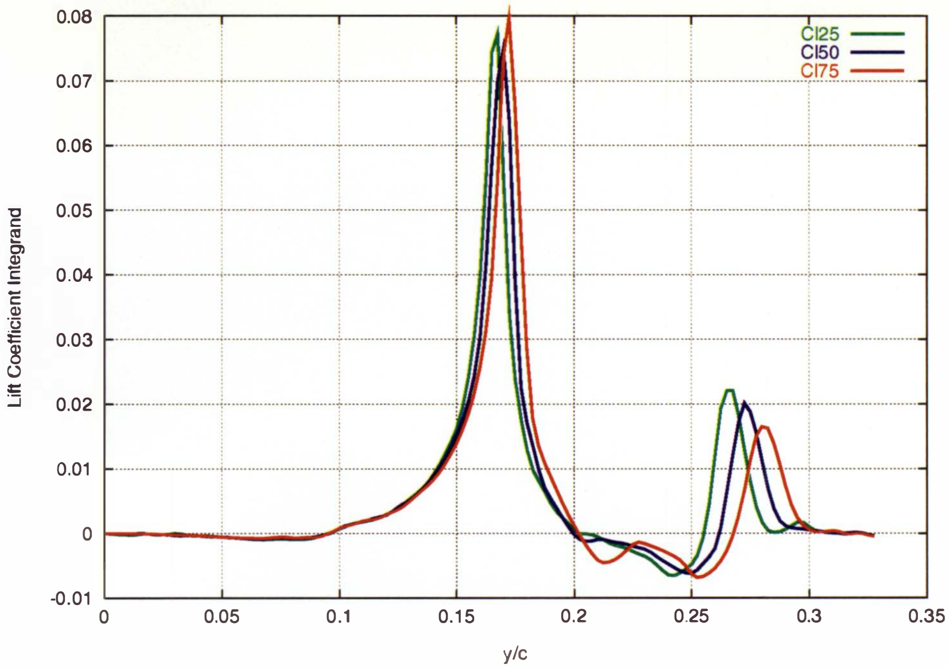

Figure 5.13: Lift Coefficients from the Three Wake Planes

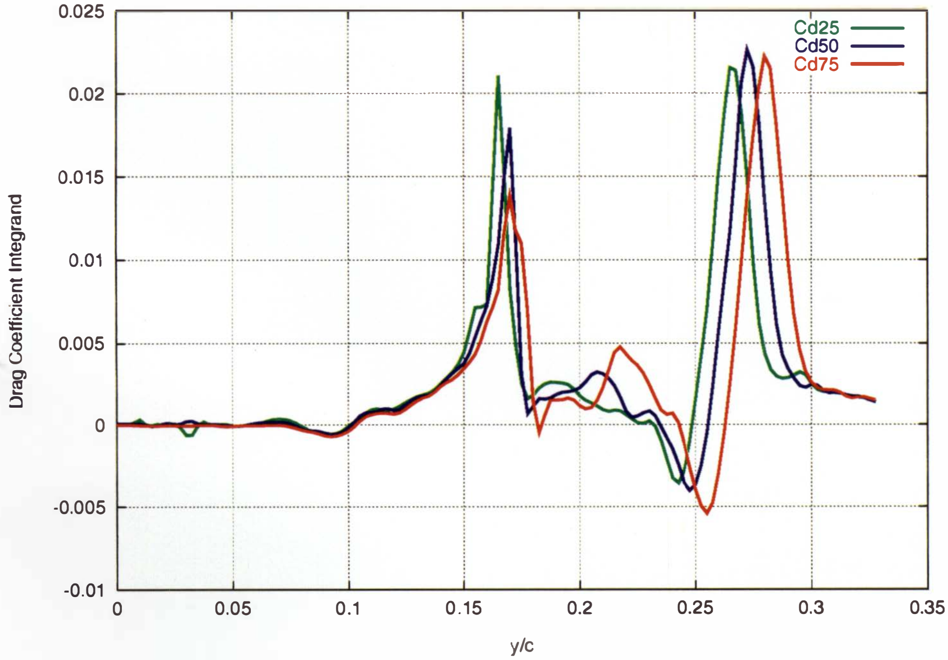

Figure 5.14: Drag Coefficients from the Three Wake Planes

Because the normal force is perpendicular to the delta wing, one can not clearly identify whether its constituents are beneficial or not. For example, positive normal force is favorable since it contributes to lift, but it is not beneficial in the sense that it creates drag. Negative normal force is good for creating thrust on the wing, but it is always unfavorable to lift. In the case of axial force, the favorable constituents are clear. Negative terms contribute to thrust and lift, and they are the ideal components. Positive ones always create drag and negative lift; therefore, they are very inefficient. If the wake plane is perpendicular to the free-stream velocity, the determination of good and bad components will be clarified, since ideally positive lift and negative drag are demanded. Therefore, to summarize the qualitative results, one should focus on a single wake-plane plot (i.e. at the wake plane $x/c = 1.075$ location) and the lift and drag span-wise distribution. From Fig.5.12, one can identify that the lift force comes mostly from the main vortex, and that additional contribution is due to the secondary vortex, which separates from the tip of the trailing edge. Further, the major drag contribution emerges partially from the secondary vortex and partially from the main vortex. Their contributions seem to be approximately the same. Relatively high aerodynamic efficiency is achieved in the main vortex region ($0.1 < y/c < 0.2$), where L/D ratio reaches approximately a value of 6. A very low, even negative ratio is in the region where $y/c > 0.2$ – the region of the largest total pressure loss (viscous drag). In order to clarify from which constituents lift and thrust benefit, one has to examine Figures 5.9 and 5.10. From Fig.5.9, the term containing axial vorticity contributes to the lift and drag from both vorticity regions, and is the dominating term. The other two vortical constituents have approximately the same effect in the main vortex region (drag and negative lift), but the term containing $C_{N_{\Omega_z}}$ also has a reversed influence in the secondary vortex region. The last term, curvature effect, has the smallest magnitude and contributes to the normal force. From Fig.5.10, the

constituent containing the axial vorticity term is the only ideal constituent, since lift and thrust benefit from both vortex regions. The remaining three terms – total pressure loss, pressure variations and curvature effect – are unfavorable, since they contribute to drag and negative lift. The total pressure loss term has an oscillatory behavior along the span, but overall it contributes to drag and negative lift. The pressure variations and the curvature effect are positive throughout most of the span location; only small regions exist where they are beneficial.

5.3 Sources of Errors

If one assumes that the experimental data and the relative position between the measured grid points have no uncertainties, then the computational errors consist of numerical errors due to finite difference approximation and due to numerical integration. For the 5−point stencil formula, the local error is

$$\frac{h^4}{30} f^{(5)}(\xi), \tag{5.1}$$

where h is the grid size, and $f^{(5)}(\xi)$ is the fifth-order derivative of a function f, evaluated at a location ξ in the domain. However, one wake plane consists of approximately $3,500$ points, and ten derivatives are evaluated at each point (five flow variables in two dimensions); therefore, global contribution, in the worst case assumption, will increase by a factor of 35×10^3. The global error, introduced by two-dimensional Simpson's rule integration, for a rectangular grid of size h is

$$-\frac{\Delta X \Delta Y h^4}{180}[f_x^{(4)}(\bar{\xi},\bar{\eta}) + f_y^{(4)}(\hat{\xi},\hat{\eta})], \tag{5.2}$$

where ΔX and ΔY is the range of the integrated region, and $f_x^{(4)}(\bar{\xi},\bar{\eta})$ and $f_y^{(4)}(\hat{\xi},\hat{\eta})$ are the fourth-order derivatives of the integrated function with respect to x and y accordingly, evaluated at some interior points.

In our example, $h = 0.005$, $\Delta X = 0.33$ and $\Delta Y = 0.25$. One can see that the error caused by the finite difference formulas has a larger contribution than the integration error. Even though a large factor was introduced to (5.1) for the global error, its coefficient is $35 \times 10^3\, h^4/30 \approx 7 \times 10^{-7}$. The error will probably be negligible compared to the total values of the lift and drag coefficients, which are $O(10^{-1})$.

In any case, all data is measured with some uncertainties; therefore, they contribute to the final computed results. Since the computation of the flow-field variable uncertainties is complicated, and since the error bands needed for such computations are not available, this procedure is omitted. However, in order to illustrate some error analysis, let f be any measured quantity in the flow field, x be the relative position between two consecutive points, and Δf and Δx be their percentage uncertainties, respectively. Then, the error due to numerical approximation of a derivative $\partial f / \partial x$ (where f can be p_0, p, u, v or w) would be $\sqrt{(\Delta f)^2 + (\Delta x)^2}$ for each term of the five-point stencil formula in (4.6), where four different uncertainties need to be substituted for Δf and Δx. Looking at (4.3) and (4.4), one can see that obtaining of x-derivative terms requires a multiplication and division; therefore, they are the source of large errors. Let Δu, Δv, Δw, and Δy be percentage errors in velocity components u, v, w and grid size h respectively. Then, the error in a single term of (4.3) or (4.4)

$$\frac{v}{u}\frac{\partial w}{\partial y} \quad \text{is} \quad \sqrt{(\Delta u)^2 + (\Delta v)^2 + (\Delta w)^2 + (\Delta y)^2}.$$

Because the x-derivative terms are used in the computation of two vorticity components and the axial force constituent, their error might be significant, even for small uncertainties in the measured flow variables. When using the numerical stencil for a derivative of an empirical function (4.5), one has to evaluate least square errors for each derivative computed, and integrate them over the whole domain. By doing this, one obtains the total least square error. The least square error is highly dependent on

the grid size, because it assumes that the curvature of the function does not change significantly over the points which are used for the computation. If the grid is not fine enough, this assumption might not be satisfied in the vortex core, and high smoothing of the derivatives will be performed in that region.

Chapter VI

Conclusion

The assumptions of the wake-plane theory were not exactly satisfied; therefore, the quantitative values obtained using the theory are not completely reliable. However, physical interpretation of the results reveal information about the role of the main and secondary vortices on the aerodynamic force of the delta wing. Constituents contributing to the normal and axial forces were also identified. This is important to an aircraft designer, since diagnostics of different wing shapes and vehicles can be studied and optimized accordingly. One could see in §5.2 that the secondary vortex was unfavorable to the aerodynamic efficiency of the delta wing; therefore, a designer should focus on eliminating this vortex by a more careful wing-tip design or, if necessary, to modify the straight line leading edge. Moreover, one could see that the aerodynamic force comes mainly from the regions of vorticity. Not only the constituents containing vorticity terms were localized to vortex regions, but also the terms containing static and total pressures. Because, to the author's knowledge, this is the first work done in applying near-wake plane surveys in such close vicinity to a model, it can not be compared to any other method. The main question, which requires more study, is under what conditions the assumptions of the theory will be met in wind-tunnel flows. It would be beneficial to obtain a numerical code for a wind-tunnel model computation, in order to carefully study the effect of the uniform-flow assumption on the side boundary of the control volume. Using such a code, the walls of the wind tunnel could be extended to an arbitrary size; therefore, the wall effect on the final result computed by the wake-plane theory could be studied. Additionally, the results obtained by a classical method of surface pressure integration could be compared to the present wake-analysis results by using such a code.

List of References

List of References

1. Durand, W.F., *Aerodynamic Theory,* Vol.3, Dover Publications, Inc., Mineola, NY 11501.

2. Maskell, E.C., "Progress Towards a Method for the Measurement of the Components of the Drag of Wing of Finite Span," Royal Aircraft Establishment Technical Report 72232, 1973.

3. Hackett, J.E. and Sugavan, A., "Evaluation of a Complete Wake Integral for the Drag of a Car-Like Shape", *SAE paper 840577*, Feb. 1984.

4. Hackett, J.E. and Sugavan, A., "Recent Developments in Three Dimensional Wake Analysis", *AGARD R-723*, July 1985.

5. Brune, G.W., "Quantitative Three-Dimensional Low-Speed Wake Surveys, " at *The Fifth Symposium on Numerical and Physical Aspects of Aerodynamic Flows*, paper *N93-27447.*

6. Brune, G.W., "Low-Speed Wake Surveys", *J. Aircraft* (1994) **31**, 249-255.

7. Takahashi, T.T. and Ross, J.C., "On the Development of an Efficient Wake Surveys System," *SAE Technical Paper 951990*, 1995.

8. Yates, J.E. and Donaldson, C. duP., "A Fundamental Study of Drag and an Assessment of Conventional Drag-Due-to-Lift Reduction Devices", *NASA CP4004*, 1986.

9. Wu, J.Z. and Wu, J.M., "Vortical Sources of Aerodynamic Force and Moment", *SAE Technical Paper 892346*, 1989.

10. Wu, J.Z. and Wu, J.M., "Interactions between Solid Surface and a Viscous Compressible Flow Field", *J. Fluid Mech.*, (1993) **254**, 183-211

11. Wu, J.Z. and Wu, J.M., "Vorticity Dynamics on Boundaries," 1996, *Adv. Appl. Mech.* **32**, edited by J.W. Hutchinson and T.Y. Wu, Academic Press.

12. Washburn, A.E., "High Angle of Attack Aerodynamics - Unsteady and Separated Flow Phenomena and Control", Short Course Notes, The University of Tennessee Space Institute, Tullahoma, TN, Sept.18-22, 1995.

13. Lanczos, C., *Applied Analysis*, Dover Publications, Inc., Mineola, NY 11501.

14. Press, W.H., Teukolsky, S.A., Vetterling, W.T. and Flannery, B.P., *Numerical Recipes in C*, Press Syndicate of the University of Cambridge, New York, NY 10011, 1992.

15. Hackett, J.E., Wilsden, D.J. and Stevens, W.A., "A Review of the Wall Pressure Signature and Other Tunnel Constraint Correction Methods For High Angle-of-Attack Tests", *AGARD R-692*, Feb. 1981.

16. Johnson, F.T., Tinoco, E.N., Lu P. and Epton, M.A., "Recent Advances in the Solution of Three-Dimensional Flows over Wings with Leading Edge Vortex Separation", *AIAA paper 79-0282*, Jan. 1979.

17. Wu, J.Z. and Wu, J.Z., "A Theoretical Formulation of Wave Vortex Interactions", *AIAA paper 89-0988* March 1989.

18. Wu, J.C., Hackett, J.E. and Lilley, D.E., "A Generalized Wake-Integral Approach for Drag Determination in Three-Dimensional Flows", *AIAA paper 79-0279*, Jan. 1979.

19. Burden, R.L. and Faires, J.D., *Numerical Analysis*, Prindle, Weber and Schmidt Publishing Company, Boston, MA 02116.

20. Schlichting, H., *Boundary Layer Theory*, 6th ed., McGraw Hill, 1968.

21. Ashley, H. and Landahl M., *Aerodynamics of Wings and Bodies*, 1985, Dover Publications, Inc., Mineola, NY 11501.

22. Pope, A. and Harper, J.J., *Low-Speed Wind Tunnel Testing*, John Wiley & Sons, Inc., 1966.

Appendix

Appendix

Derivation of the Incompressible Lift Formula

Assuming a constant density in (2.9), the equation can be rearranged as follows.

$$\begin{aligned}
L_{inc} &= \int_T y\left[\frac{\partial}{\partial y}(\rho u w) - \frac{\partial}{\partial z}(\rho u v)\right] dS \\
&= \int_T \rho y\left[\frac{\partial}{\partial y}(u w) - \frac{\partial}{\partial z}(u v)\right] dS \\
&= \int_T \rho y\left[u\frac{\partial w}{\partial y} + w\frac{\partial u}{\partial y} - u\frac{\partial v}{\partial z} - v\frac{\partial u}{\partial z}\right] dS \\
&= \int_T \rho y\left[u(\frac{\partial w}{\partial y} - \frac{\partial v}{\partial z}) - v(\frac{\partial u}{\partial z} - \frac{\partial w}{\partial x}) + w(\frac{\partial u}{\partial y} - \frac{\partial v}{\partial x}) - v\frac{\partial w}{\partial x} + w\frac{\partial v}{\partial x}\right] dS \\
&= \int_T \rho y\left[u\omega_x - v\omega_y - w\omega_z + w\frac{\partial v}{\partial x} - v\frac{\partial w}{\partial x}\right] dS
\end{aligned}$$

The above formula can also be re-written as follows

$$L_{inc} = \int_T \rho y\left[u\omega_x - (v\omega_y + w\omega_z) + w^2\frac{\partial}{\partial x}(\frac{v}{w})\right] dS \qquad (1)$$

Derivation of the Compressible Lift Formula

An additional term, due to density variations, has to be added to the above formula, which is

$$L_\rho = \int_T yu[w\frac{\partial}{\partial y} - v\frac{\partial}{\partial z}]\rho dS.$$

Assuming a perfect gas with constant specific heats, the entropy may be expressed as

$$\begin{aligned}
s &= c_p \ln\left(\frac{T}{T_r}\right) - R\ln\left(\frac{p}{p_r}\right) = c_p \ln\left(\frac{T}{T_r}\right) - R\ln\left(\frac{\rho T}{\rho_r T_r}\right) \\
&= (c_p - R)\ln\left(\frac{T}{T_r}\right) - R\ln\left(\frac{\rho}{\rho_r}\right) = c_v \ln\left(\frac{T}{T_r}\right) - R\ln\left(\frac{\rho}{\rho_r}\right)
\end{aligned}$$

where T_r, p_r and ρ_r are constant reference values corresponding to $s_r = 0$. Taking a derivative of s with respect to y, one obtains

$$\frac{\partial s}{\partial y} = c_v\frac{\partial(\ln T)}{\partial y} - R\frac{\partial(\ln \rho)}{\partial y}$$

$$
\begin{aligned}
&= \frac{c_v}{T}\frac{\partial T}{\partial y} - \frac{R}{\rho}\frac{\partial \rho}{\partial y} \\
&= \frac{c_v}{c_p T}\frac{\partial h}{\partial y} - \frac{R}{\rho}\frac{\partial \rho}{\partial y},
\end{aligned}
$$

from which

$$
\frac{\partial \rho}{\partial y} = \rho \frac{c_v}{c_p R T}\frac{\partial h}{\partial y} - \frac{\rho}{R}\frac{\partial s}{\partial y} = \frac{\rho}{\gamma R T}\frac{\partial h}{\partial y} - \frac{\rho}{R}\frac{\partial s}{\partial y}.
$$

Similarly, a derivative with respect to z can be obtained. Using formula $\gamma R T = a^2$, where a is the speed of sound, the compressible part of lift becomes

$$
\begin{aligned}
L_\rho &= \int_T yuw\frac{\partial \rho}{\partial y}dS - \int_T yuv\frac{\partial \rho}{\partial z}dS \\
&= \int_T \rho yuw\left[\frac{1}{a^2}\frac{\partial h}{\partial y} - \frac{1}{R}\frac{\partial s}{\partial y}\right]dS - \int_T yuv\left[\frac{1}{a^2}\frac{\partial h}{\partial z} - \frac{1}{R}\frac{\partial s}{\partial z}\right]dS \\
&= \int_T \rho yu\frac{1}{a^2}\left[w\frac{\partial}{\partial y} - v\frac{\partial}{\partial z}\right]hdS - \int_T yuv\frac{1}{R}\left[w\frac{\partial}{\partial y} - v\frac{\partial}{\partial z}\right]sdS \\
&= \int_T \rho y M_x\left[M_z\frac{\partial}{\partial y} - M_y\frac{\partial}{\partial z}\right]hdS - \int_T y\gamma T M_x\left[M_z\frac{\partial}{\partial y} - M_y\frac{\partial}{\partial z}\right]sdS
\end{aligned}
$$

Therefore, the compressible lift formula is

$$
L_{comp} = L_{inc} + L_\rho. \tag{2}
$$

Derivation of the Incompressible Drag Formula

Assuming constant density in (2.7), the equation can be rearranged as follows

$$\begin{aligned} D_{inc} &= \frac{1}{k}\int_{\mathcal{T}}(y\frac{\partial}{\partial y}+z\frac{\partial}{\partial z})(p+\rho u^2)dS \\ &= \frac{1}{k}\int_{\mathcal{T}}\boldsymbol{x}\cdot\boldsymbol{\nabla}_\pi p dS+\frac{2}{k}\int_{\mathcal{T}}\rho u[(z\omega_y-y\omega_z)+\frac{\partial}{\partial x}(\boldsymbol{x}\cdot\boldsymbol{u}_\pi)]dS, \end{aligned}$$

where the following formula was used:

$$\begin{aligned} (y\frac{\partial}{\partial y}+z\frac{\partial}{\partial z})u^2 &= 2u(y\frac{\partial}{\partial y}+z\frac{\partial}{\partial z})u \\ &= 2u(y\frac{\partial u}{\partial y}+z\frac{\partial u}{\partial z}) \\ &= 2u(y\frac{\partial u}{\partial y}-y\frac{\partial v}{\partial x}+z\frac{\partial u}{\partial z}-z\frac{\partial w}{\partial x}+y\frac{\partial v}{\partial x}+z\frac{\partial w}{\partial x}) \\ &= 2u[y(-\omega_z)+z\omega_y+\frac{\partial}{\partial x}(\boldsymbol{x}\cdot\boldsymbol{u}_\pi)] \\ &= 2u[(z\omega_y-y\omega_z)+\frac{\partial}{\partial x}(\boldsymbol{x}\cdot\boldsymbol{u}_\pi)]. \end{aligned}$$

For incompressible flows, the Crocco's equation can be used

$$\boldsymbol{\nabla} p_0=\rho(\boldsymbol{u}\times\boldsymbol{\omega}).$$

Dotting the above equation with a position vector only in the $\mathcal{T}$-plane, one obtains

$$\begin{aligned} \boldsymbol{x}\cdot\boldsymbol{\nabla}_\pi p_0 &= \rho[y(w\omega_x-u\omega_z)+z(u\omega_y-v\omega_x)] \\ &= \rho[u(z\omega_y-y\omega_z)+\omega_x(yw-zv)], \end{aligned}$$

or

$$u(z\omega_y-y\omega_z)=\frac{1}{\rho}\boldsymbol{x}\cdot\boldsymbol{\nabla}_\pi p_0+\omega_x(zv-yw)$$

Therefore, the total drag for incompressible flows can be expressed as

$$\begin{aligned} D_{inc} &= \frac{1}{k}\int_{\mathcal{T}}\boldsymbol{x}\cdot\boldsymbol{\nabla}_\pi p dS+\frac{2}{k}\int_{\mathcal{T}}\boldsymbol{x}\cdot\boldsymbol{\nabla}_\pi p_0 dS \\ &+ \frac{2}{k}\int_{\mathcal{T}}\rho[\omega_x(zv-yw)+u\frac{\partial}{\partial x}(\boldsymbol{x}\cdot\boldsymbol{u}_\pi]dS \end{aligned} \quad (3)$$

Derivation of the Compressible Drag Formula

Including the density variations in (2.7), one obtains

$$
\begin{aligned}
D &= \frac{1}{k}\int_{\mathcal{T}}(y\frac{\partial}{\partial y}+z\frac{\partial}{\partial z})(p+\rho u^2)dS \\
&= \frac{1}{k}\int_{\mathcal{T}}(\boldsymbol{x}\cdot\boldsymbol{\nabla}_\pi p+\rho\boldsymbol{x}\cdot\boldsymbol{\nabla}_\pi u^2+u^2\boldsymbol{x}\cdot\boldsymbol{\nabla}_\pi\rho)dS. \qquad (4)
\end{aligned}
$$

By using formulas

$$
\boldsymbol{\nabla} h_0=\boldsymbol{u}\times\boldsymbol{\omega}+T\boldsymbol{\nabla} s \qquad \text{and} \qquad \boldsymbol{\nabla} h=\frac{\boldsymbol{\nabla} p}{\rho}+T\boldsymbol{\nabla} s,
$$

the total drag can be expressed in terms of enthalpy h, entropy s and velocity field $\boldsymbol{u}$.

$$
\boldsymbol{\nabla} p=\rho\boldsymbol{\nabla} h-\rho T\boldsymbol{\nabla} s \qquad \Longrightarrow \qquad \boldsymbol{x}\cdot\boldsymbol{\nabla}_\pi p=\rho\boldsymbol{x}\cdot\boldsymbol{\nabla}_\pi h-\rho T\boldsymbol{x}\cdot\boldsymbol{\nabla}_\pi s
$$

Dotting the stagnation enthalpy term with the position vector in $\mathcal{T}$-plane only, one gets

$$
\begin{aligned}
\boldsymbol{x}\cdot\boldsymbol{\nabla}_\pi h_0 &= \boldsymbol{x}\cdot(\boldsymbol{u}\times\boldsymbol{\omega})_\pi+T\boldsymbol{x}\cdot\boldsymbol{\nabla}_\pi s \\
&= y(w\omega_x-u\omega_z)+z(u\omega_y-v\omega_x)+T\boldsymbol{x}\cdot\boldsymbol{\nabla}_\pi s \\
&= \omega_x(yw-zv)+u(z\omega_y-y\omega_z)+T\boldsymbol{x}\cdot\boldsymbol{\nabla}_\pi s
\end{aligned}
$$

and

$$
u(z\omega_y-y\omega_z)=\boldsymbol{x}\cdot\boldsymbol{\nabla}_\pi h_0-T\boldsymbol{x}\cdot\boldsymbol{\nabla}_\pi s-\omega_x(yw-zv)
$$

Using the previous result for the incompressible drag

$$
\boldsymbol{x}\cdot\boldsymbol{\nabla}_\pi u^2=2[u(z\omega_y-y\omega_z)+u\frac{\partial}{\partial x}(\boldsymbol{x}\cdot\boldsymbol{u}_\pi)]
$$

one can determine the following quantity to be

$$
\rho\boldsymbol{x}\cdot\boldsymbol{\nabla}_\pi u^2 = 2\rho[\boldsymbol{x}\cdot\boldsymbol{\nabla}_\pi h_0-T\boldsymbol{x}\cdot\boldsymbol{\nabla}_\pi s-\omega_x(yw-zv)+u\frac{\partial}{\partial x}(\boldsymbol{x}\cdot\boldsymbol{u}_\pi)]
$$

The last term in (4), due to density variations, is

$$
\begin{aligned}
\boldsymbol{x}\cdot\boldsymbol{\nabla}_\pi\rho &= (y\frac{\partial}{\partial y}+z\frac{\partial}{\partial z})\rho=y\frac{\partial\rho}{\partial y}+z\frac{\partial\rho}{\partial z} \\
&= y\left[\frac{\rho}{\gamma RT}\frac{\partial h}{\partial y}-\frac{\rho}{R}\frac{\partial s}{\partial y}\right]+z\left[\frac{\rho}{\gamma RT}\frac{\partial h}{\partial z}-\frac{\rho}{R}\frac{\partial s}{\partial z}\right] \\
&= \frac{\rho}{\gamma RT}\left(y\frac{\partial}{\partial y}+z\frac{\partial}{\partial z}\right)h-\frac{\rho}{R}\left(y\frac{\partial}{\partial y}+z\frac{\partial}{\partial z}\right)s,
\end{aligned}
$$

and

$$u^2 \boldsymbol{x} \cdot \boldsymbol{\nabla}_\pi \rho = \rho M_x^2 \boldsymbol{x} \cdot \boldsymbol{\nabla}_\pi h - \rho \gamma T M_x^2 \boldsymbol{x} \cdot \boldsymbol{\nabla}_\pi s$$

Substituting all constituents into (4) the total compressible drag becomes

$$\begin{aligned} D_{comp} &= \frac{2}{k}\int_T \rho \boldsymbol{x} \cdot \boldsymbol{\nabla}_\pi h_0 dS + \frac{1}{k}\int_T \rho(1 + M_x^2)\boldsymbol{x} \cdot \boldsymbol{\nabla}_\pi h dS \\ &- \frac{1}{k}\int_T \rho T(3 + \gamma M_x^2)\boldsymbol{x} \cdot \boldsymbol{\nabla}_\pi s dS \\ &+ \frac{2}{k}\int_T \rho[\omega_x(zv - yw) + u\frac{\partial}{\partial x}(\boldsymbol{x} \cdot \boldsymbol{u}_\pi)]dS. \end{aligned} \tag{5}$$

VITA

Bohus Ondrusek was born in Nova Dubnica, Slovakia on January 8, 1966. He attended a secondary school in Slovakia, from which he graduated in May, 1985. In December, 1986, he emigrated to the United States, where he held various jobs for the first three years. He then began his university studies, graduating from Boston University in May 1994, having earned a degree in Aerospace Engineering. In the fall of 1994, he entered The University of Tennessee Space Institute as a graduate student and a research assistant.

He enjoys various kinds of winter and summer sports, his favorite being downhill skiing and windsurfing. He also likes to travel, camp and hike in the mountains.